Master Thesis

Theoretical investigations on the influence of artificially induced joints on the performance of mechanical rock excavation by roadheaders

Stefan Rudolf Bock, BSc.

Lehrstuhl für Bergbaukunde, Bergtechnik und Bergwirtschaft
Department Mineral Resources Engineering
Montanuniversität Leoben

A-8700 LEOBEN, Franz Josef Straße 18
Tel.Nr.: +43 3842-402-2001
Fax: +43 3842-402-2002
bergbau@unileoben.ac.at

eidesstattliche Erklärung / Affidavit

Ich erkläre an Eides statt, dass ich diese Arbeit selbstständig verfasst, andere als die angegebenen Quellen und Hilfsmittel nicht benutzt und mich auch sonst keiner unerlaubten Hilfsmittel bedient habe.

I declare in lieu of oath, that I wrote this thesis and performed the associated research myself, using only literature cited in this volume.

……………………………….. ……………………………….

Date   Signature

Acknowledgment

I want to thanks my adviser Mr. Dipl.-Ing. Dr.mont Philipp Hartlieb for the excellence scientific advises during all project phases.

Abstract

The influence of the specific energy to the cutting performance was investigated and different hybrid cutting performance perdition models were established. Those models vary in different cutting depths and different preconditioning depths of the tunnel face. The most effective forecast model of Mr. Comakli was investigated in more detail.

These multi regression models sets the uniaxial compressive strength, Brazilian tensile strength, Schmidt hammer value, ultrasonic test, dry density and porosity into relation. The original equation creates a correlation value of 0.98.

As the best precondition technique the microwave fragmentation was chosen, because the horizontal and radial cracks create an easier situation for extraction of the tunnel face with a roadheader cutting head than e.g vertical laser drilled holes. Lower the rock mass rating by a factor of 20% will lead to an improvement of the performance, expressed by the net cutting rate of 22%.

The preconditioning with laser drilled holes (vertical and inclined) was interpreted as not sufficient for mining operations, because the tunnel face will get too hot and the thermal wear of the wolframite pick will move out of the economic situation.

The most effective cutting situation could be a microwave preconditioned face and a water jet assisted cutting process. As best the precondition will be, as higher the cutting performance will be in the end.

Zusammenfassung

In this thesis several material testing techniques and rock rating parameters were presented. These input parameters influence the cutting performance of roadheaders in a very intense way. The specific energy of rock turned into the special focus of this master thesis.

Also different alternative fragmentation technics were discussed for applying those in mining operations. As last chapter several forecast models were compared and discussed.

List of content

1 Roadheaders

Underground roadheaders were heavy-duty equipment for tunneling and drift excavation operations. The top range for excavating minerals can reach up to a uniaxial compression strength of 120 MPa. Beyond that strength the excavation gets uneconomic in reaction of very high tool erosion. The excavation process can be carried out by trans or axial cutting heads, where hard metal cutting picks are mounted.

The installed power can reach up to 547 kW (manufacture Sandvik (N.N, Sandvik). The average loading capacity is 350 m³/h. The cutting power can reach up to 325 kW.

To cut higher ranges of UCSs, different hybrid cutting techniques have to be researched.

In this paper cutting rocks up to UCSs 250 MPa has been investigated. The provided mechanical cutting power for the hybrid cutting models is 300 kW.

Figure 1: Roadheader Sandvik (www.sandvik.com)

1.1 Cutting characteristics

1.1.1 Chip formation

As reaction to increasing cutting forces, the stress between the rock pick and the rock surface rises up until the rock strength is reached (boarder between elastic and plastic stress situation).

Celal wrote in his paper in the year 2013 that after this first stage lateral and median cracks run through the plastic deformation zone.

As second stage the lateral cracks reach the surface, in a circle like way. Here the maximum of cutting force is reached.

As last stage of the cutting process, the chips are moved out by the rock pick (crushed zone). For this only the shear resistance has to be overcome. All the described processes can be seen in Figure 2 below.

For very ductile rocks shear forces will dominate the chipping process, on the other side for very brittle process lateral and median cracks dominate the process.
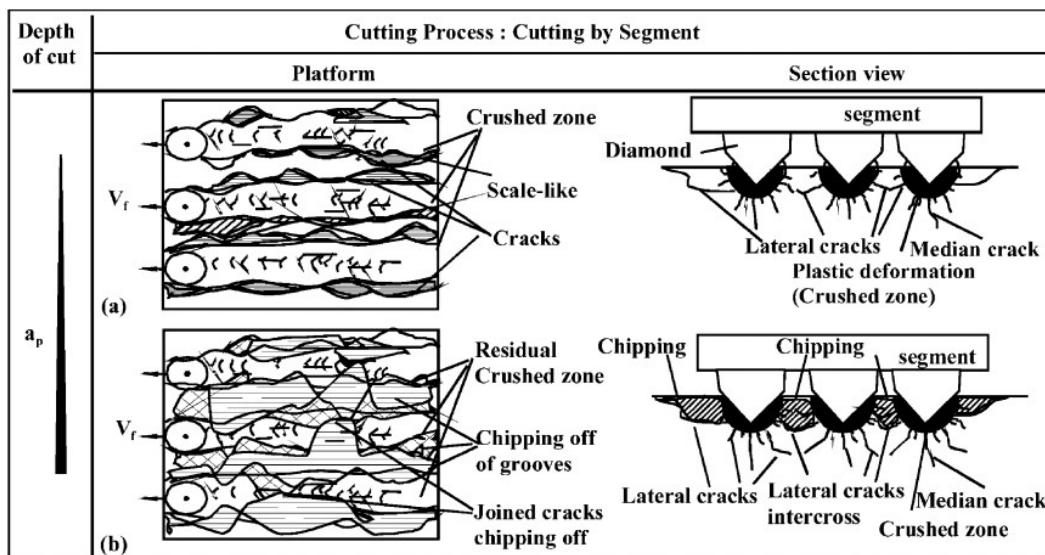
Figure 2: Cutting process (Pihtili 2013)

1.1.2 Angle influence to cutting forces

To induce a higher efficiency during cutting operations, it is necessary to control the forces and angles of attack to the excavating material. Those parameters were presented in Figure 3.
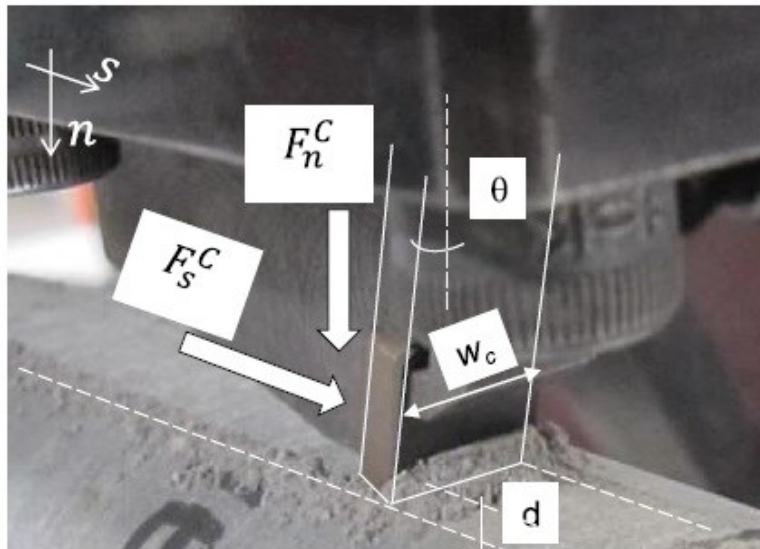
Figure 3: Geometric conditions during cutting process (Munoz et al. 2016)

The geometric designations were:

d… cutting depth W_c…cutting width F_s^C…peak cutting force

F_n^C…normal cutter force to surface   θ… angle of cutter

Munoz et al wrote in their paper (2016) that the cuttability indices are influenced by:

- rock texture
- grain size
- UCS
- Mohrs hardness
- structural parameters
- tool-rock interactions (friction losses)

In their paper they investigate θ for 15°, 30° and 45° over different cutting depths.

The results at low cutting depths showed plastic yielding (material fails by yield stress).

At deeper cutting depth the fracture mode will be dominant.

The nominal stress is shown in the equation below after the size effect law (Bazant´s law):

$$\sigma_n = \frac{(F_s^c)_{peak}}{w_c \times d} \qquad (1)$$

Figure 4 shows the influence of the cutting depth to the necessary cutting forces. The letter ε represents the specific energy (SE).

The Mantina stands for basalt, Brukunga for phylite and Hawksbury for sandstone minerals.
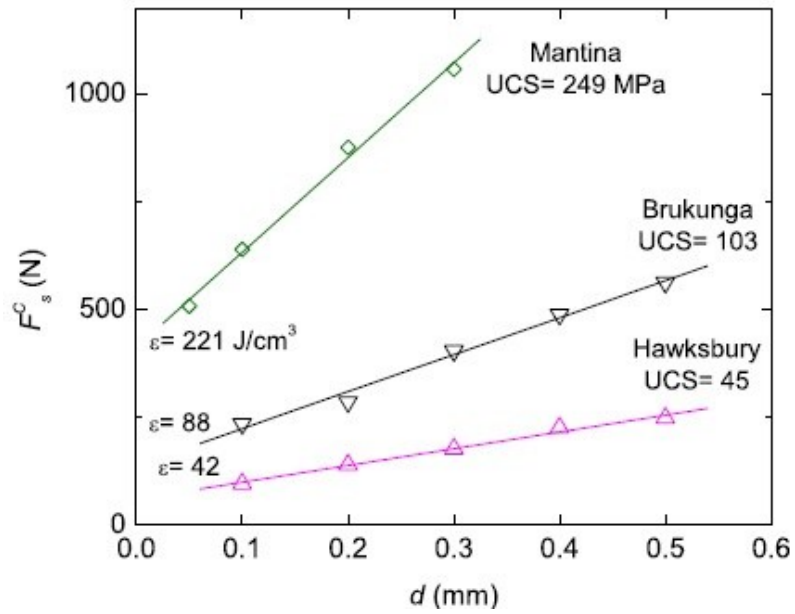
Figure 4: Cutting force over cutting depth (Munoz et al. 2016)

For example, the cutting experiment (Figure 5) of Brukunga shows the influence of θ:
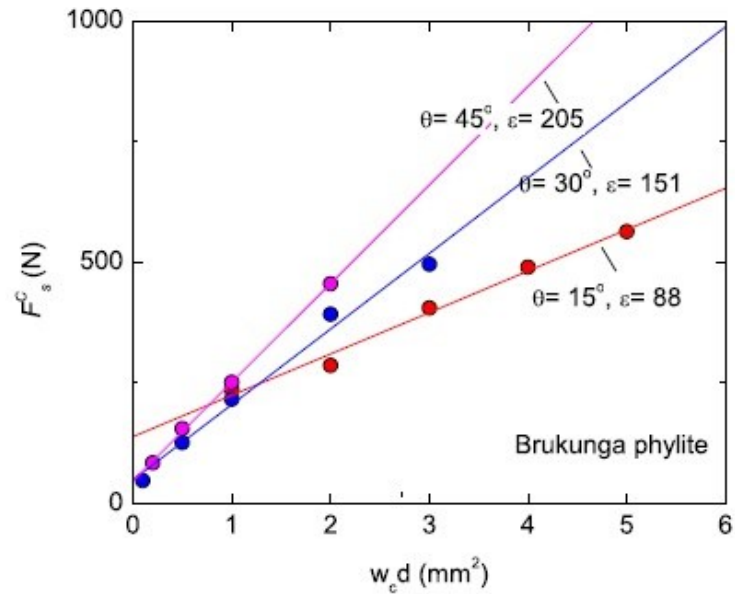
Figure 5: Brukunga cutting test (Munoz et al. 2016)

The SE for this were at a constant w_c= 10mm

θ=15°	88 J/cm³
θ=30°	151 J/cm³
θ=45°	205 J/cm³

The conclusion of the Munoz et al experiment was that a higher attack angle causes a higher amount of SE to excavate the same amount of material.

2 Rock mass classification models

The aim of rock classification models is to give forecast information about the rock properties during the feasibility and preliminary design stage of a mining/tunneling project. During this stage of preliminary reconnaissance no detailed information (UCS, BTS, CAI, …) are available.

The prediction models cannot replace the laboratory research activities of rock (mass) properties during the construction stage.

In the following sector of the thesis different classification models are presented.

Hoeck recommended a short list of the common models which are used in the mining industry:

- Rock Quality Designation Index (RQD)
- Rock Structure Rating (RSR)
- Rock mass rating (RMR)
- Barton (Q-Value)
- Geological Strength Index (GSI)

Normally serval classification models were applied at the same face to give a more detailed view of the rock properties (and also to compare them).

Most use in practice are Bienawskies RMR and Bartons Q-Value rock mass ratings.

2.1.1 Rock Quality Designation Index (RQD)

This drill core quality rating was invented by Deere et al in the year 1967. The RQD is defined as the percentage of unbroken pieces, which are longer than 100mm, of a drill core. The equation below shows this relation:

$$RQD = \frac{\sum_i^n length\ of\ pieces\ longer\ than\ 100\ mm}{total\ length\ of\ core} \qquad (2)$$

Hoeck mentioned that this value is strongly depending on the orientation of the drilled hole. Joints and discontinuities can influence the value in an intense way.

Figure 6 shows a short example:
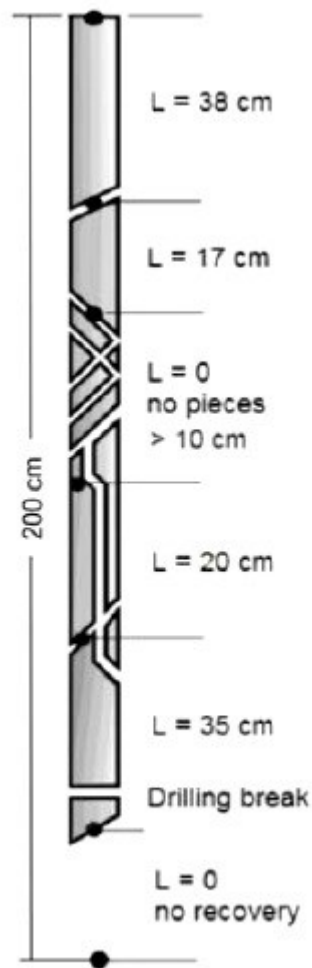

Figure 6: RQD (Hoek)

The RQD Value of this core sample using the equation above
RQD = (380+170+200+350) / 2000 = 55%

2.1.2 Rock Structure Rating (RSR)

This method to rate rock mass was invented by Wickham et al (1972). An advantage of this method is that the classification of the necessary support is included. Equation 2 shows the rating:

$$RSR = A + B + C \qquad (3)$$

Parameter A represents the estimation of the geology and geological structures (see Table 1)

Parameter B represents the influence of discontinuities on the tunnel orientation (see Table 2)

Parameter C represents the influence of ground water (inflow and joint condition) (see Table 3)

Table 1: RSR Parameter A (Hoek)

	Basic Rock Type					Geological Structure		
	Hard	Medium	Soft	Decomposed				
Igneous	1	2	3	4		Slightly	Moderately	Intensively
Metamorphic	1	2	3	4		Folded or	Folded or	Folded or
Sedimentary	2	3	4	4	Massive	Faulted	Faulted	Faulted
Type 1					30	22	15	9
Type 2					27	20	13	8
Type 3					24	18	12	7
Type 4					19	15	10	6

Table 2: RSR Parameter B (Hoek)

	Strike ⊥ to Axis					Strike ‖ to Axis		
	Direction of Drive					Direction of Drive		
	Both	With Dip		Against Dip		Either direction		
		Dip of Prominent Joints [a]				Dip of Prominent Joints		
Average joint spacing	Flat	Dipping	Vertical	Dipping	Vertical	Flat	Dipping	Vertical
1. Very closely jointed, < 2 in	9	11	13	10	12	9	9	7
2. Closely jointed, 2-6 in	13	16	19	15	17	14	14	11
3. Moderately jointed, 6-12 in	23	24	28	19	22	23	23	19
4. Moderate to blocky, 1-2 ft	30	32	36	25	28	30	28	24
5. Blocky to massive, 2-4 ft	36	38	40	33	35	36	24	28
6. Massive, > 4 ft	40	43	45	37	40	40	38	34

Table 3: RSR Parameter C (Hoek)

	Sum of Parameters A + B					
	13 - 44			45 - 75		
Anticipated water inflow	Joint Condition [b]					
gpm/1000 ft of tunnel	Good	Fair	Poor	Good	Fair	Poor
None	22	18	12	25	22	18
Slight, < 200 gpm	19	15	9	23	19	14
Moderate, 200-1000 gpm	15	22	7	21	16	12
Heavy, > 1000 gp	10	8	6	18	14	10

[a] Dip: flat: 0-20°; dipping: 20-50°; and vertical: 50-90°
[b] Joint condition: good = tight or cemented; fair = slightly weathered or altered; poor = severely weathered, altered or open

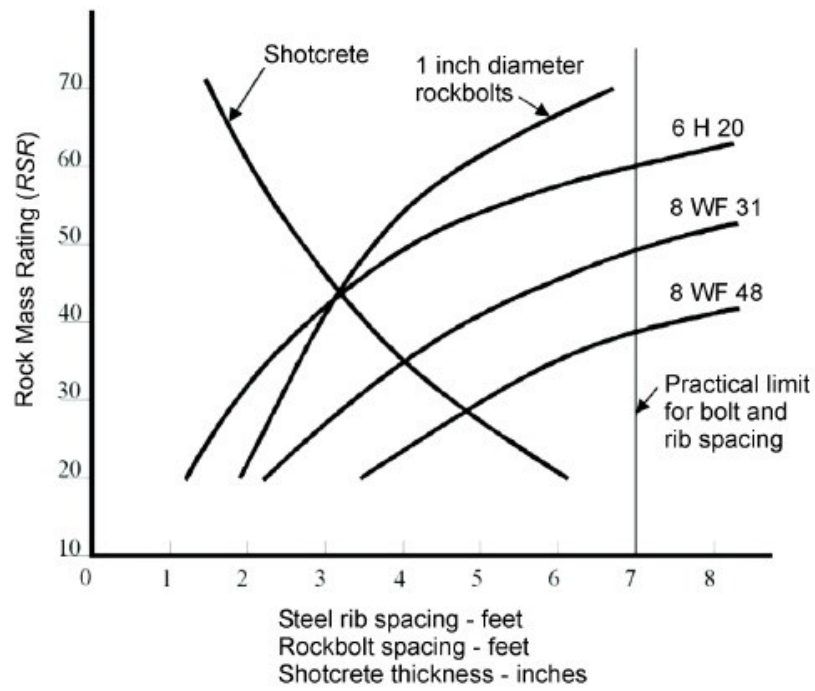After calculation the RSR the support can be read out of Figure 7

Figure 7: RSR Support (Hoek)

For example, a RSR of 60 will create a minimum support of 2.2 inches (5.6 cm) of shotcrete in addition with 1-inch diameter rockbolts spaced every 4.5 feet (1.4 m).

2.1.3   Rock Mass Rating (RMR)

This method was invented by Bieniawski in the year 1976 and modified in the year 1989.

The model after Hoek rates the following parameters to a maximum sum of 100:

1. UCS of material
2. RQD
3. Spacing of the discontinuities
4. Condition of the discontinuities
5. Water conditions
6. Orientation of discontinuities

Table 5 shows the detailed information about the rating of the parameters. All parameters can be rated directly in situ, except the strength values (Point Load and UCS).

The result of the rating can directly be read out of Table 4.

Table 4: results of Bieniawski rating (Hoek)

Rock mass class	Excavation	Rock bolts (20 mm diameter, fully grouted)	Shotcrete	Steel sets
I - Very good rock RMR: 81-100	Full face, 3 m advance.	Generally no support required except spot bolting.		
II - Good rock RMR: 61-80	Full face , 1-1.5 m advance. Complete support 20 m from face.	Locally, bolts in crown 3 m long, spaced 2.5 m with occasional wire mesh.	50 mm in crown where required.	None.
III - Fair rock RMR: 41-60	Top heading and bench 1.5-3 m advance in top heading. Commence support after each blast. Complete support 10 m from face.	Systematic bolts 4 m long, spaced 1.5 - 2 m in crown and walls with wire mesh in crown.	50-100 mm in crown and 30 mm in sides.	None.
IV - Poor rock RMR: 21-40	Top heading and bench 1.0-1.5 m advance in top heading. Install support concurrently with excavation, 10 m from face.	Systematic bolts 4-5 m long, spaced 1-1.5 m in crown and walls with wire mesh.	100-150 mm in crown and 100 mm in sides.	Light to medium ribs spaced 1.5 m where required.
V – Very poor rock RMR: < 20	Multiple drifts 0.5-1.5 m advance in top heading. Install support concurrently with excavation. Shotcrete as soon as possible after blasting.	Systematic bolts 5-6 m long, spaced 1-1.5 m in crown and walls with wire mesh. Bolt invert.	150-200 mm in crown, 150 mm in sides, and 50 mm on face.	Medium to heavy ribs spaced 0.75 m with steel lagging and forepoling if required. Close invert.

Table 5: Rock Mass Rating System (Hoek)

A. CLASSIFICATION PARAMETERS AND THEIR RATINGS

	Parameter		Range of values					
1	Strength of intact rock material	Point-load strength index	>10 MPa	4 - 10 MPa	2 - 4 MPa	1 - 2 MPa	For this low range - uniaxial compressive test is preferred	
		Uniaxial comp. strength	>250 MPa	100 - 250 MPa	50 - 100 MPa	25 - 50 MPa	5 - 25 MPa	1 - 5 MPa	< 1 MPa
	Rating		15	12	7	4	2	1	0
2	Drill core Quality RQD		90% - 100%	75% - 90%	50% - 75%	25% - 50%	< 25%	
	Rating		20	17	13	8	3	
3	Spacing of		> 2 m	0.6 - 2. m	200 - 600 mm	60 - 200 mm	< 60 mm	
	Rating		20	15	10	8	5	
4	Condition of discontinuities (See E)		Very rough surfaces. Not continuous. No separation. Unweathered wall rock	Slightly rough surfaces. Separation < 1 mm. Slightly weathered walls	Slightly rough surfaces. Separation < 1 mm. Highly weathered walls	Slickensided surfaces or Gouge < 5 mm thick or Separation 1-5 mm Continuous	Soft gouge >5 mm thick or Separation > 5 mm Continuous	
	Rating		30	25	20	10	0	
5	Groundwater	Inflow per 10 m tunnel length (l/m)	None	< 10	10 - 25	25 - 125	> 125	
		(Joint water press)/ (Major principal σ)	0	< 0.1	0.1, - 0.2	0.2 - 0.5	> 0.5	
		General conditions	Completely dry	Damp	Wet	Dripping	Flowing	
	Rating		15	10	7	4	0	

B. RATING ADJUSTMENT FOR DISCONTINUITY ORIENTATIONS (See F)

Strike and dip orientations		Very favourable	Favourable	Fair	Unfavourable	Very Unfavourable
Ratings	Tunnels & mines	0	-2	-5	-10	-12
	Foundations	0	-2	-7	-15	-25
	Slopes	0	-5	-25	-50	

C. ROCK MASS CLASSES DETERMINED FROM TOTAL RATINGS

Rating	100 ← 81	80 ← 61	60 ← 41	40 ← 21	< 21
Class number	I	II	III	IV	V
Description	Very good rock	Good rock	Fair rock	Poor rock	Very poor rock

D. MEANING OF ROCK CLASSES

Class number	I	II	III	IV	V
Average stand-up time	20 yrs for 15 m span	1 year for 10 m span	1 week for 5 m span	10 hrs for 2.5 m span	30 min for 1 m span
Cohesion of rock mass (kPa)	> 400	300 - 400	200 - 300	100 - 200	< 100
Friction angle of rock mass (deg)	> 45	35 - 45	25 - 35	15 - 25	< 15

E. GUIDELINES FOR CLASSIFICATION OF DISCONTINUITY conditions

Discontinuity length (persistence) Rating	< 1 m 6	1 - 3 m 4	3 - 10 m 2	10 - 20 m 1	> 20 m 0
Separation (aperture) Rating	None 6	< 0.1 mm 5	0.1 - 1.0 mm 4	1 - 5 mm 1	> 5 mm 0
Roughness Rating	Very rough 6	Rough 5	Slightly rough 3	Smooth 1	Slickensided 0
Infilling (gouge) Rating	None 6	Hard filling < 5 mm 4	Hard filling > 5 mm 2	Soft filling < 5 mm 2	Soft filling > 5 mm 0
Weathering Ratings	Unweathered 6	Slightly weathered 5	Moderately weathered 3	Highly weathered 1	Decomposed 0

F. EFFECT OF DISCONTINUITY STRIKE AND DIP ORIENTATION IN TUNNELLING**

Strike perpendicular to tunnel axis		Strike parallel to tunnel axis	
Drive with dip - Dip 45 - 90°	Drive with dip - Dip 20 - 45°	Dip 45 - 90°	Dip 20 - 45°
Very favourable	Favourable	Very unfavourable	Fair
Drive against dip - Dip 45-90°	Drive against dip - Dip 20-45°	Dip 0-20 - Irrespective of strike°	
Fair	Unfavourable	Fair	

* Some conditions are mutually exclusive . For example, if infilling is present, the roughness of the surface will be overshadowed by the influence of the gouge. In such cases use A.4 directly.
** Modified after Wickham et al (1972).

2.1.4 Rock Tunneling Quality Index (Q-Value)

Another very prominent method is the Q-Value which was invented by in the year Barton, Lien and Lunde (1974). The equation below shows the relation of several parameters:

$$Q = \frac{RQD}{Jn} \times \frac{Jr}{Ja} \times \frac{Jw}{SRF} \qquad (4)$$

RQD   Rock Quality Designation

Jn   joint set number

Jr   joint roughness number

Ja   joint alteration number

Jw   water reduction factor

SRF   stress reduction factor

The logarithmic results of the equation can be directly put into Figure 8. Out of this diagram the rock classes (A-G) and information about the support categories can be read out.
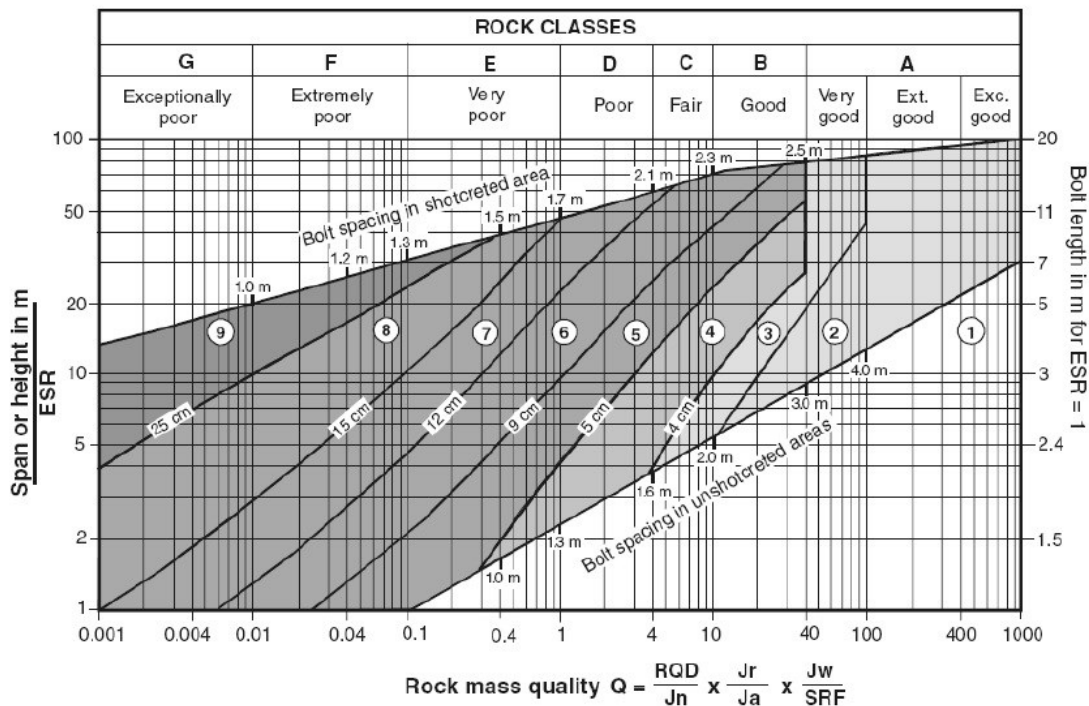
Figure 8: RQD support categories (Hoek)

2.1.5 Geological Strength Index (GSI)

The last method to geological rating of the rock masses is the GSI-Value, which was invented by Hoek and Brown (1997).

It is a visual interpretation of the tunnel-face in tunneling operations, or surface of bench in open pit mining operations. Figure 9 shows the template for the rock mass evaluation.

After Marinos typical ranges for various rock types varies between ranges of:

- Sandstone massive / brecciated: 90-45 / 45-30
- Siltstone, Claystone bedded / sheared: 45-22 / 25-5
- Limestone massive / thin bedded / brecciated: 90-45 / 56-34 / 45-27
- Granite: 90-50
- Ultrabasic rocks fresh / serpentinised: 90-38 / 25-8
- Gneiss: 90-35
- Schist strong / weak / sheared: 58-40 / 40-16 / 25-7
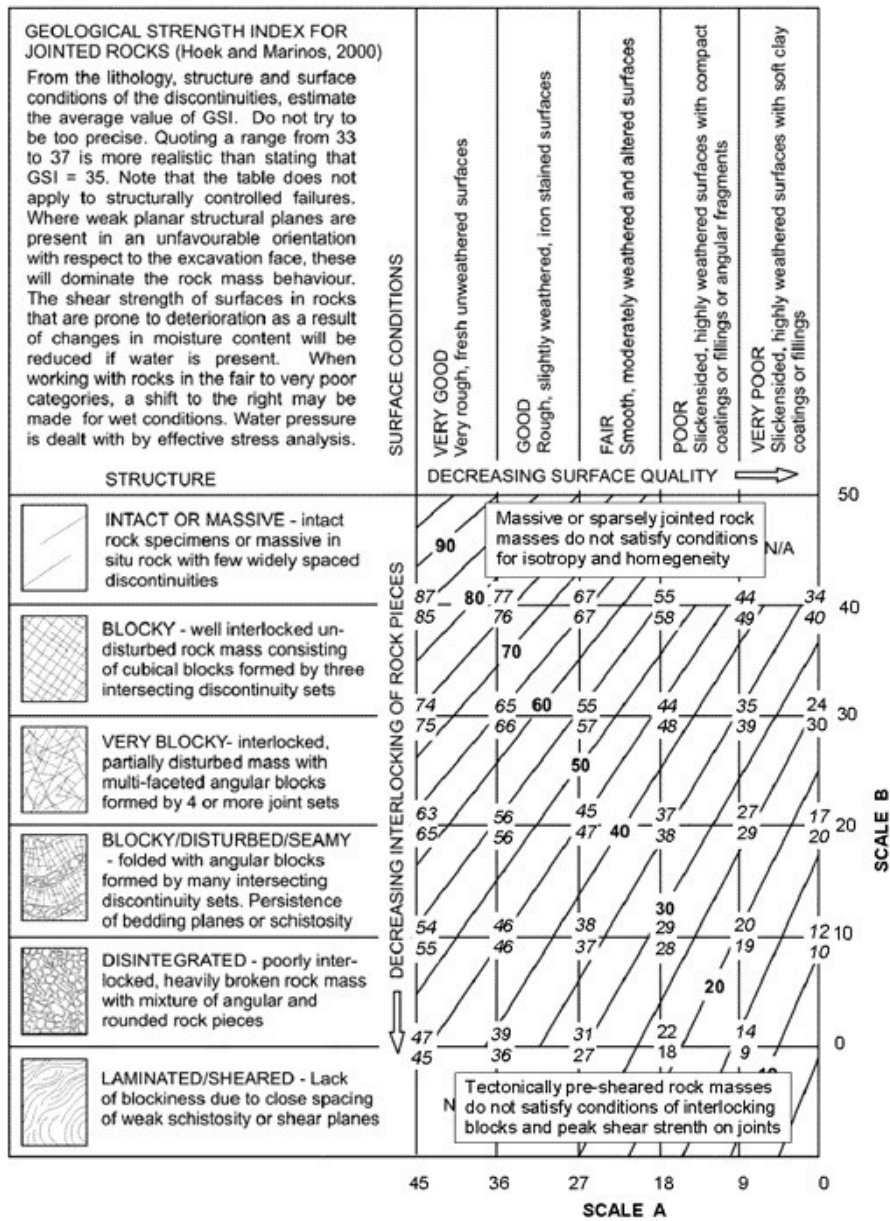
Figure 9: GSI Value (Hoek, Carter, Diederichs 2013)

2.2 Material testing

2.2.1 Uniaxial compressive strength

The uniaxial compressive strength (UCS) is one of the most used parameters in mining engineering.

The UCS is defined as the stress of a sample during the failure situation during the testing procedure. The equation below shows the mathematical term:

$$\sigma = \frac{F_{max}}{A} \qquad (\text{kN/mm}^2) \qquad (5)$$

Restner wrote in his master thesis (1998), that there were two testing conditions. Those conditions are: stability and cuttability.

Stability:

• water flushing is allowed

• weaker parts of the rock

• low loading rates ($\sigma(t) \leq$ 5MPa/min)

• large, slim specimens (height/diameter $\approx$ 2)

Cuttability:

• dry sampling is to be preferred

• stronger parts of the rock

• high loading rates ($\sigma(t) \geq$ 600 MPa/min)

• small, cubic specimens (height/diameter $\approx$ 1)

Figure 10 shows the sample during the testing.

Figure 10: UCS testing device

Table 6 will show the UCS of several rock types.

Table 6 UCS Strength (after Solenhofen, 2003)

Rock type	UCS (MPa)
Granite	100-250
Diabase	150-300
Basalt	100-300
Sandstone	20-170
Limestone	30-250
Dolomit	30-250
Steel	900-1500

2.2.2 Brazilian tensile test

The Brazilian tensile test investigate indirectly the tensile strength of a sample.

Under pressure the sample collapses along the Y-axis (see Figure 11). The strength of the sample gets calculated with the equation below.

$$\sigma_t = \frac{2 \times F}{\pi \times D \times t} \qquad (6)$$

F…maximal load on sample   D… diameter of sample   t…thickness of sample
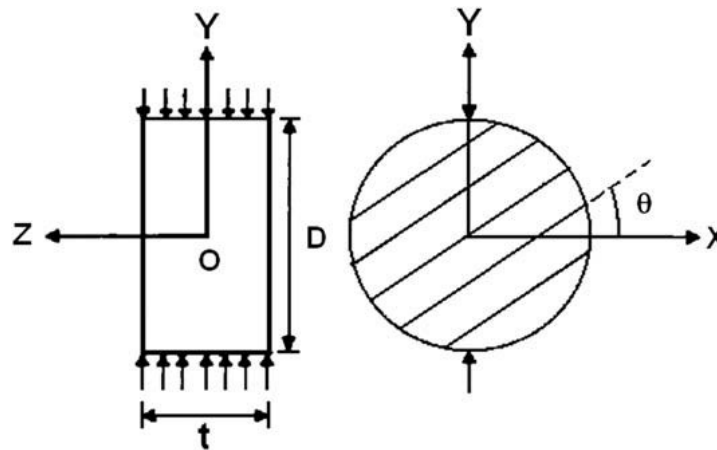
Figure 11: Brazilian tensile test (Tavallali und Vervoort 2010)

,,
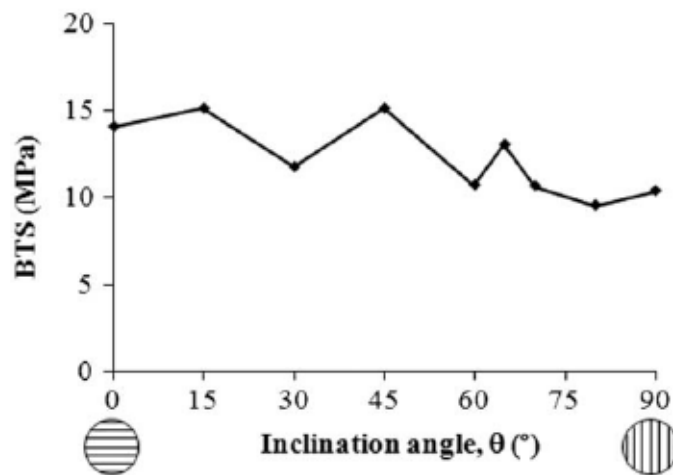
Figure 12: influence of inclination angle to BTS (Tavallali und Vervoort 2010)

Tavallali und Vervoort wrote in their paper (2010), that for limestone the BTS varies between 14 - 36 MPa.

For crosschecking of the results the BTS should be approximately 10 % of the UCS results.

2.2.3 Brittleness test

This indirect testing procedure was published by Yagiz and Gokceoglu (2010) and is deriving the brittleness out of the rock strength (punch penetration test). The experimental arrangement is presented in Figure 13. The specimen diameter is 54 mm, the height to diameter ration has to be at least 1. For this test it is necessary to fix the sample into a steel ring (inner diameter of 115 mm) with gypsum to create a high resistance against yielding. The penetration procedure ends automatically at a penetration of 6.5 mm. The constant penetration speed is 0.0254 mm/s.
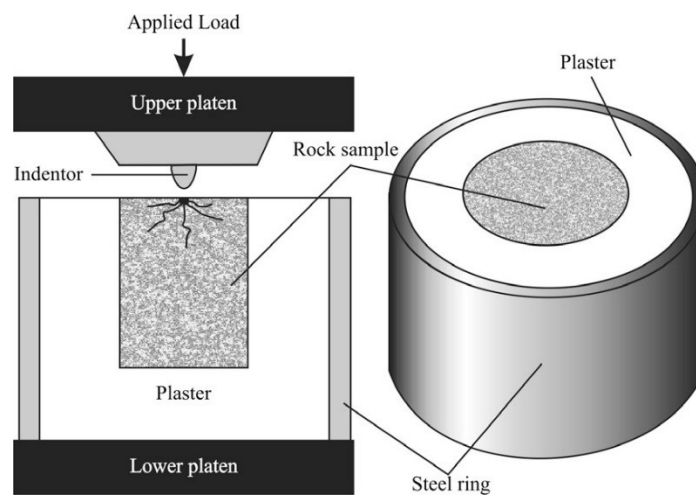
Figure 13: punch penetration test (Yagiz and Gokceoglu 2010)

Out of the force-penetration diagram (Figure 14) the brittleness can be calculated.

$$BI_m = \frac{F_{max}}{P} \qquad (7)$$

F_{max} …maximal penetrating force (kN) P …penetration at maximal force (mm)
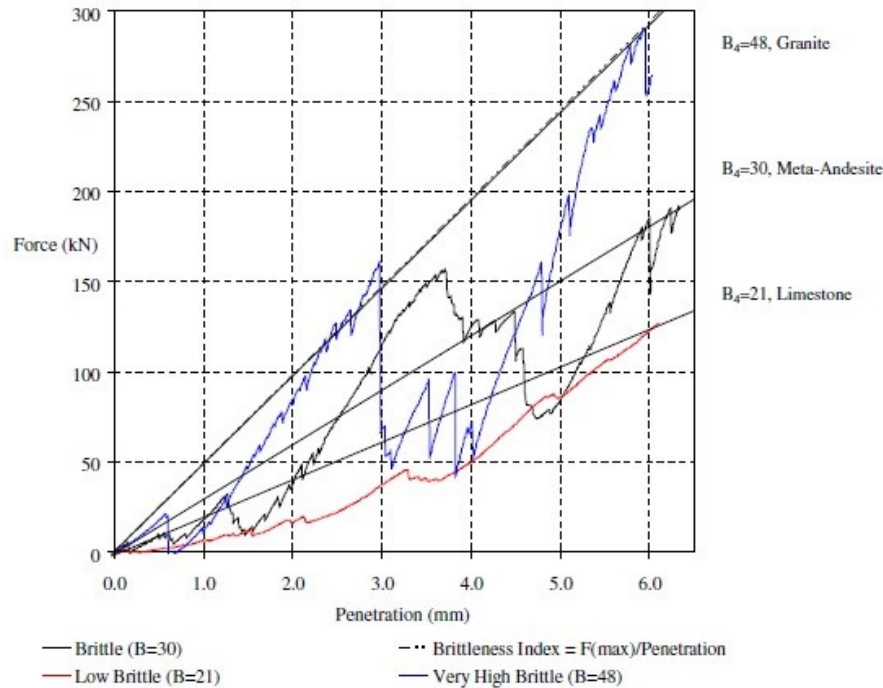
Figure 14: Brittleness graph (Yagiz and Gokceoglu 2010)

As classification of the results the following ranges (kN/mm)

≥40 very high brittle	35-39 high brittle	30-34 medium brittle
25-29 moderate brittle	20-24 low brittle	≤19 not brittle (ductile)

Several rock types are listed below to give a little overview (all rocks were from USA):

Sandstone: 10.7-30.5	Limestone 14-35.7	Gneiss 17.4-36.8
Granite 27.0-41.7	Basalt 21.0-42	Marble 35

Yagiz and Gokceoglu also investigated a multiple linear regression between the rock parameters of compressive strength (σ_c in MPa), tensile strength (σ_t in MPa) and the specific weight (ρ in kN/m³). The equation below shows this relation:

$$BI_M = 0.198 \times \sigma_c - 2.174 \times \sigma_t + 0.913 \times \rho - 3.807 \qquad (8)$$

This equation creates a correlation coefficient (R^2) of 0.94

2.2.4 Cerchar abrasiveness

The third important material testing parameter in this thesis, is the abrasiveness index after Cerchar (researched in the year 1986). The experimental principal is shown in Figure 15.

The scratch distance of the pin is 10 mm and the load during the test is 70 N.

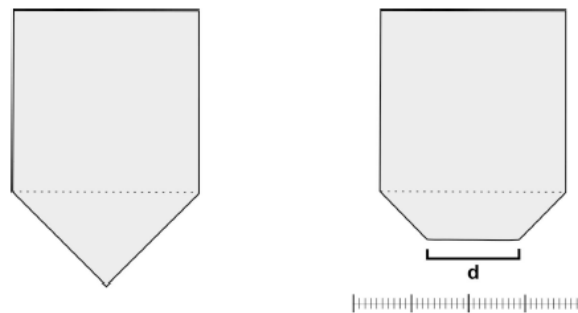After the test the diameter of the plane pin top is measured.

Figure 15: Cerchar experimental principle (Käsling 2010)

The Index (CAI) gets calculated out of the equation below:

$$CAI = 10 * \frac{d}{c} \quad (9)$$

c… unit correction factor (standard 1 mm)

Table 7: CAI-Index (after Käsling 2010)

CAI-Index	category	material
<0.3	not abrasive	organic material
0.3-0.5	not very abrasive	mudstone, marl
0.5-1.0	slightly abrasive	slate, limestone
1.0-2.0	medium abrasive	schist, sandstone
2.0-4.0	very abrasive	basalt, quarzitic sandstone
>4.0	extremely abrasive	Amphibolite, quartzite

2.2.5 Shore hardness test

The aim of the shore hardness test in an early stage of a project is to estimate roughly the strength of a rock sample. The device below (Figure 16) shows the very basic testing situation for rock. A diamond dipped hammer impacts on the surface of the sample from a selected height. The average rebound height of 20 test is measured and calculated with the equation below into UCS. Figure 17 shows the influence of SSH to UCS of several minerals. Those minerals were: limestone, marble, basalt and sandstone.

$$UCS = 2.88 \times SSH \qquad (10)$$

SSH…shore scleroscope hardness
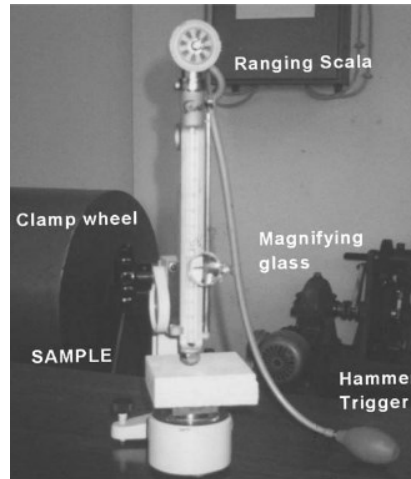
Figure 16: shore hardness test device (Yasar und Erdogan 2004)
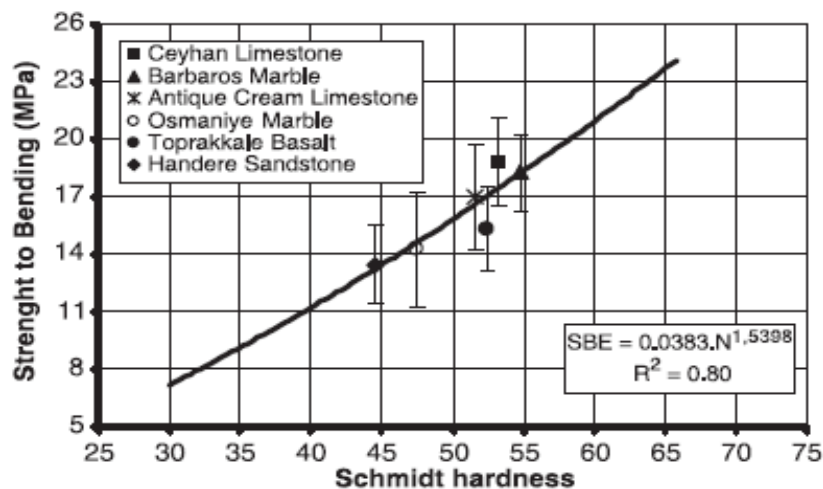
Figure 17: correlation SSH to UCS (Yasar and Erdogan, 2003)

3   Influence of rock parameters on cutting performance

For excavating operations with roadheaders, the cutting performance is the most important parameter.

The cutting performance is governed after Thuro (2002) by two input parameters. On one hand by the cuttability of the rock, which is defined by the excavation of solid rock masses per (net) working hour (m³/h). On the other hand, the cutting performance is influenced by the pick consumption per solid rock mass during excavation (picks/m³).
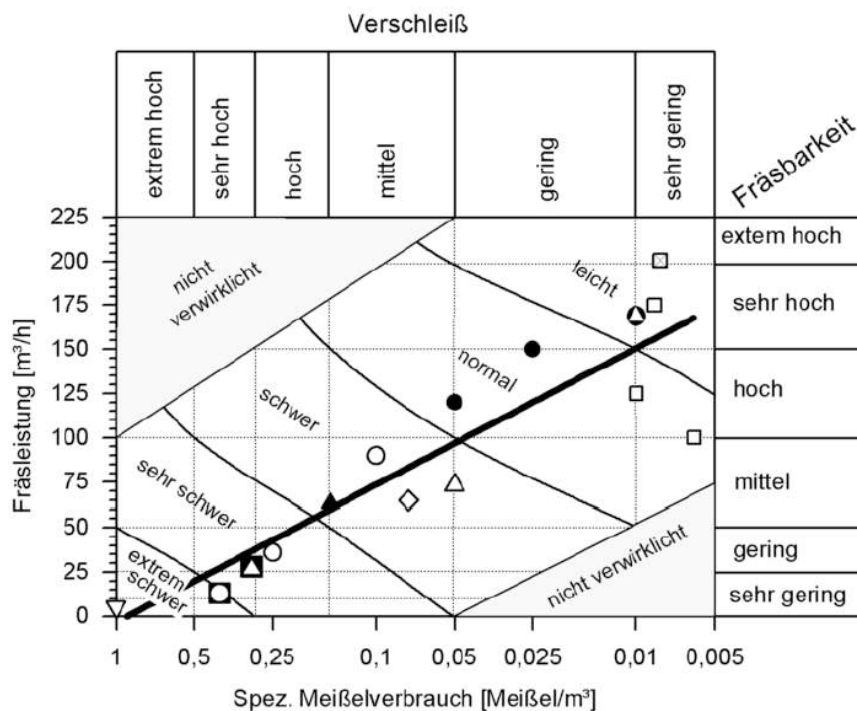

Figure 18: cutting performance for roadheaders (Thuro 2002)

Figure 18 shows a matrix for estimating the cutting performance (here "Fräsbarkeit") as a function of specific pick consumption. The range starts by very low 25 m³/h (sehr gering) and reaches to extreme high by 225 m³/h (extrem hoch). This matrix was made for a roadheader with 300 kW cutting power.

Special rock parameters can influence the cuttability of rock and the pick consumption. The list below shows some of these parameters:

- specific destruction energy
- uniaxial compressive strength
- Brazilian tensile strength
- geotechnical abrasivity

For the specific destruction energy, it is necessary to take into consideration that the post-failure energy also influences the cuttability.

Further also the joint system and the geological condition of the face influence directly the cutting performance. Figure 19 demonstrates this in a very visual diagram.
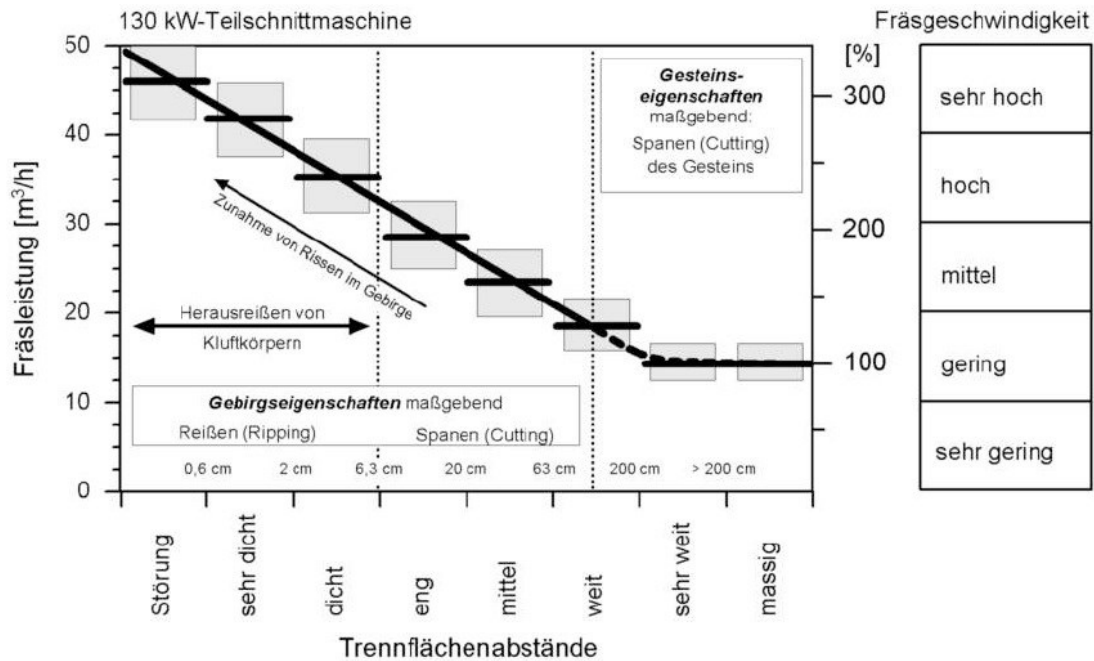

Figure 19: Cutting performance versus geological jointing (Thuro 2002)

The spacing varies between displacement (Störung) to massive (massig) face conditions. This figure was made for a 130 kW (cutting power) roadheader.

Thuro wrote in his paper 2002 that in the diagram two dominant areas can be concluded. On one hand the high energy consumption of the cutting sequence. On the other hand, the more effective ripping area. Some rock parts can get easier ripped off along those micro joints.

Also the preconditioning of the face influences the performance in a positive way.

3.1 Influence of anisotropy

The influence of anisotropy to UCS and destruction energy (which can be calculated out of the same laboratory test) will be presented in this section of the thesis. The cylindrical core samples would get drilled in different orientation to the joint system.

Thuro and Plininnger wrote in their paper (2002), that the highest UCS can be measured rectangular to the joint system. On the parallel orientation it reaches 80% to 90% of the rectangular value.

Typically the distribution graph (left side of Figure 20) shows a minimum compressive strength at an angle of 60° (out of the horizontal level). The reason of that is the missing surrounding support pressure (σ_3=0) during the test procedure.

The minimum UCS is important to investigate when the excavation direction will be diagonally to the joint system. The tensile strength shows the same analogy (right side of Figure 20). The continuous line shows a high degree of anisotropy, the broken line a strong anisotropy.
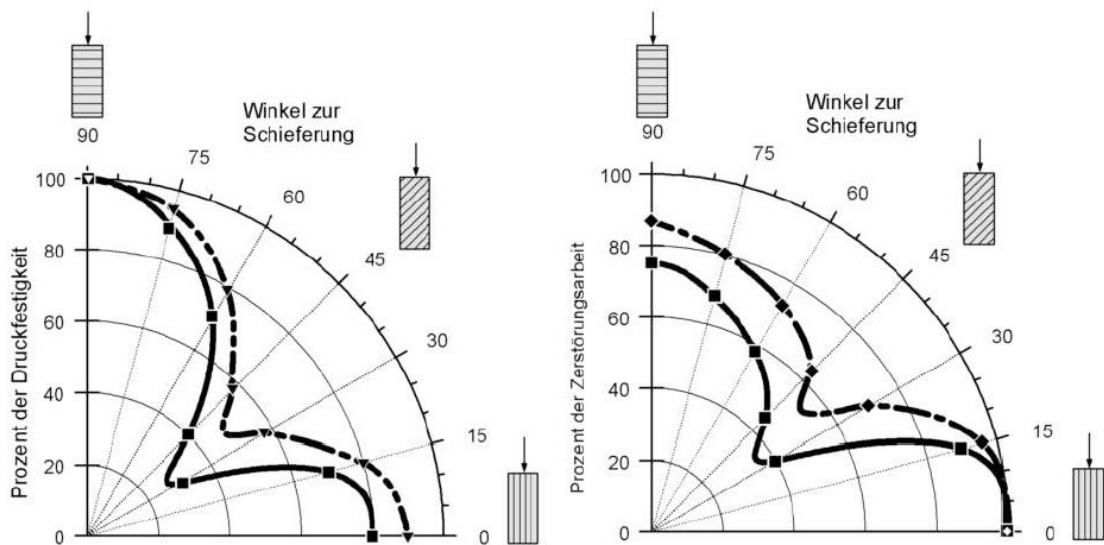

Figure 20: Anisotropy influence of UCS and tensile strength (Thuro and Plininnger)

Figure 21 shows the anisotropic influence to the cutting performance. The cutting direction parallel to the joint system creates the highest cutting performance. The lowest cutting performance of 80% to 60% ("Prozent der Fräsleistung") is found rectangular to the jointing system. The continuous line shows the performance for clay shale, the broken line shows the performance for silt saltes.
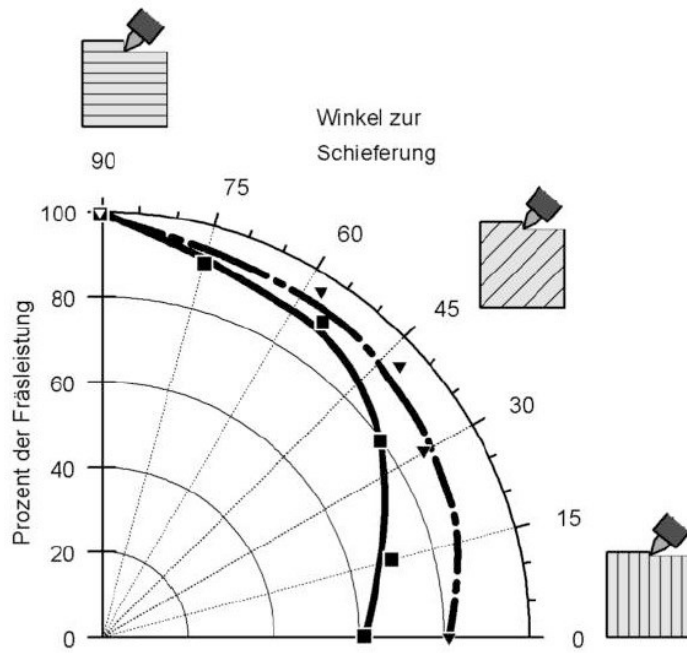
Figure 21: Anisotropic influence to cutting performance (Thuro and Plinninger)

A rectangular joint system creates also bad operation conditions for the pick tools (vibrations).

The pick tool consumption will be explained in the next chapter of this thesis.

3.2 Pick consumption

The pick consumption prediction creates a very complex problem. Especially the interaction of tool, rock mass, drilling fluid, air and rock chips is a very difficult forecast situation.

To describe the tool consumption two parameters are important.

The first parameter will be the qualitative pick consumption, which describes how the erosion of the tool is progressing in the field. It´s a visual comparison of different erosion types.

The second parameter will be the quantitative pick consumption, which describes the speed of pick erosion.

3.2.1   Qualitative pick erosion

Thuro and Plinninger wrote in their paper (2002) that all influencing factors could be compared by four different erosion parameters:

- abrasiveness (contact between tool and rock surface)
- brittle failure (erosion in result of impact stress)
- thermal wear (creates much higher erosion of the two factors above)
- special erosion (contact between tool and fluid/ aerosol media)

Figure 22 shows the characteristics of those four parameters.

Typ A: normal abrasiveness

Typ B: brittle failure
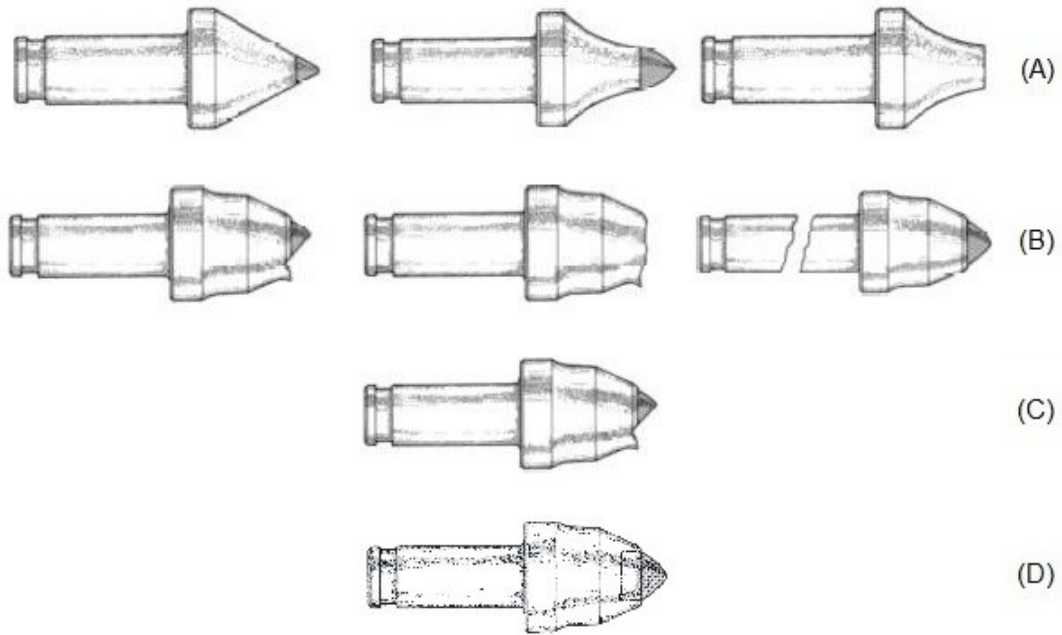
Typ C: thermal wear

Typ D: new pick

Figure 22: Qualitative pick erosion; normal abrasiveness (A), brittle failure (B), thermal wear (C), new pick (D) (Thuro and Plinninger)

In prospect to microwave-pre-conditioning thermal pick erosion is also taken into consideration. An economic operation temperature below 360°C should be issued.

3.2.2 Quantitative pick erosion

Thuro and Plinninger wrote in their paper (2002), that their erosion data are based on field data and were created in cooperation with geologists and engineers. It should work accurately for estimating the quantitative pick erosion.

Table 8 below categorize the quantitative pick erosion. The left column shows the grade of erosion. Starting on the top at very low and ends at the bottom at extreme high. In the center column the specific pick consumptions picks/m³ (solid) are listed. In the right column the pick-operation-times are presented.

Table 8: Quantitative pick erosion (after Thuro and Plinninger)

Grade of erosion	Specific pick consumption (Pick/m³)	Standup time
Very low	<0.01	Very high
low	0.01 – 0.05	High
intermediate	0.05 – 0.15	Intermediate
high	0.15 – 0.3	Low
Very high	0.3 – 0.5	Very low
Extrem high	> 0.5	Extrem low

3.3 Forecast models for performance prediction

3.3.1 Ocak and Bilgin model

The roadheader excavation performance and roadheader excavation efficiency is influenced by the factors of utilization time, as well by the net cutting rate (NCR).

The equations below were published by Ocak and Bilgin in the year 2010.

For axial type roadheaders:

$$RMCI = USC * \left(\frac{RQD}{100}\right)^{2/3} \qquad (11)$$

$$NCR = 0.28 * P * (0.974)^{RMCI} \qquad (12)$$

RMCI stands for rock mass cuttability index. UCS for the uniaxial compression strength in MPa. RQD for the rock quality designation index in %. P for the cutting power in kW and NCR for net cutting rate in m³/h.

For transversal type roadheaders:

$$RPI = P * \frac{W}{UCS} \qquad (13)$$

$$NCR = 27.11 * e^{(0.0023*RPI)} \qquad (14)$$

RPI… roadheader penetration index   W… mass of the roadheader (t).

The data have been determined empirically based on a installed cutting power of 300 kW (brand: Westfalia) and a mass of 74 tons. The average RQD was 55 % and the UCS varies between 40 - 145 MPa.

The data correlation between UCS and NCR is shown in Figure 23 below. Figure 24 presents the deviation of field data from predicted data.

The following figures were made for a rock mass mixture of sandstone, siltstone, claystone, mudstone and shale. Also limestone and conglomerates appear sometimes in the direction of the excavation.
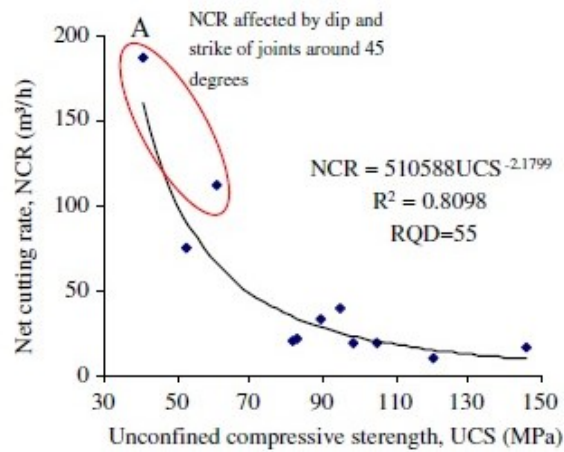
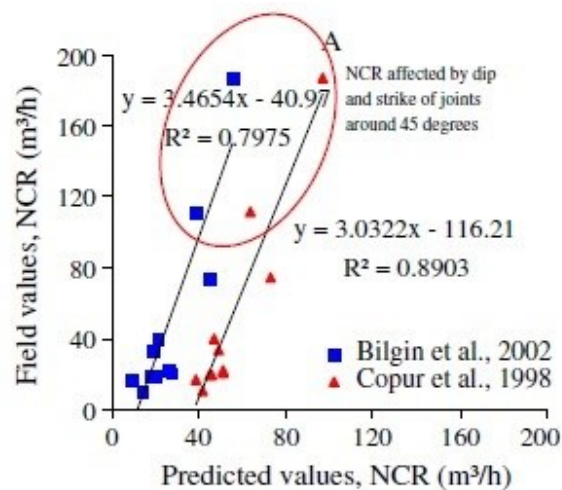*Figure 23: Relation between UCS and NCR (Ocak 2010)*

Figure 24: Deviation of field data to predicted data of NCR (Ocak 2010)

The high deviation of the NCR in Area A was created by an inclined joint system at the tunnel face. This influence were described in chapter 3.1 before. In this specific case the inclining of the joint system at 45° was very favorable for the excavation.

3.3.2 Comakli model

Comakli, Kahraman, Balci wrote in their paper (2014), that a roadheader could produce a three times higher production rate than the excavation applying traditional drilling and blasting technics. Their model was invented for metallic ores: chromite, hematite, galena and smithsonite.

The instantaneous cutting rate (ICR) is again:

$$ICR = k * \frac{P}{SE} \qquad (15)$$

P… installed cutting power (kW)   SE…specific Energy (kWh/m³)

Comakli et al declared that the energy transfer ratio factor k will be 0.8.

To estimate the specific energy several rock parameters have to be investigated.

Their model was designed for metallic ore excavation and includes several parameters (including their fluctuation range):

- uniaxial compressive strength MPa: 66.3 – 7.9

- Brazilian tensile strength MPa: 7.5 – 1.1

- point load test MPa: 3.0 – 0.5

- Schmidt hammer value: 37.9 – 15.5

- ultrasonic velocity km/s: 5.7 – 2.5

- dry density test g/cm³: 6.3 – 2.4

- dry and saturated porosity test %: 31.4 – 2.0

The results create several single-linear equations for different rock conditions:

$$SE = 1.98 * e^{0.182 * \sigma_c} \qquad (16)$$

$$SE = 1.68 * e^{0.181 * \sigma_t} \qquad (17)$$

$$SE = 1.31 * e^{0.25 * V_p} \qquad (18)$$

$$SE = -1.28 * \ln(n) + 6.74 \qquad (19)$$

The correlation coefficient drops from 0.82 to 0.51. To get better correlation coefficients a multiple linear regression model was developed. The results of this is shown in equation below. The correlation coefficient of this equation is 0.98.

$$SE = 56.1 - 0.16 * \sigma_c + 4.24 * \sigma_t - 1.08 * R_n - 0.99 * V_p - 6.43 * \rho - 0.34 * n$$

(20)

Comakli et al created another easier, but not as a good (correlation coefficient 0.75) as the equations above, equation:

$$SE = -14.9 - 0.40 * R_n - 1.78 * \rho \qquad (21)$$

In situ conditions (joint system, water, inclining, experience of the operator, stress…) can increase or decrease the cutting performance.

3.3.3 Tiryaki model I

This forecast model was invented by Tiryaki (2008). It uses a multiple nonlinear regression model to estimate the specific energy during excavation. Tiryaki wrote that tougher rocks will primary fail in shear-stress-mode and brittle rocks will fail primary in tensile-stress-mode. The process of failure and fracturing is descripted in chapter 1.1.1 .

This model was invented for 44 not specified rock types.

The testing parameter to calculate the SE in this model are listed (including their fluctuation range):

- quarz content %: 0 - 99
- dry density g/cm³: 2.2 – 2.7
- effective porosity %: 0 – 22.9
- Brazilian tensile strength MPa: 1 – 10.3
- modulus of elasticity GPa: 5.6 – 65.7
- uniaxial compressive strength MPa: 7 – 192.9
- cone indenter hardness: 1.3 - 12

The calculation with the software MATLAB creates the equation below as result of three important parameters:

$$SE = 2.15 * UCS^{0.24} * CI^{0.68} \qquad (22)$$

The correlation coefficient of this equation is 0.84.

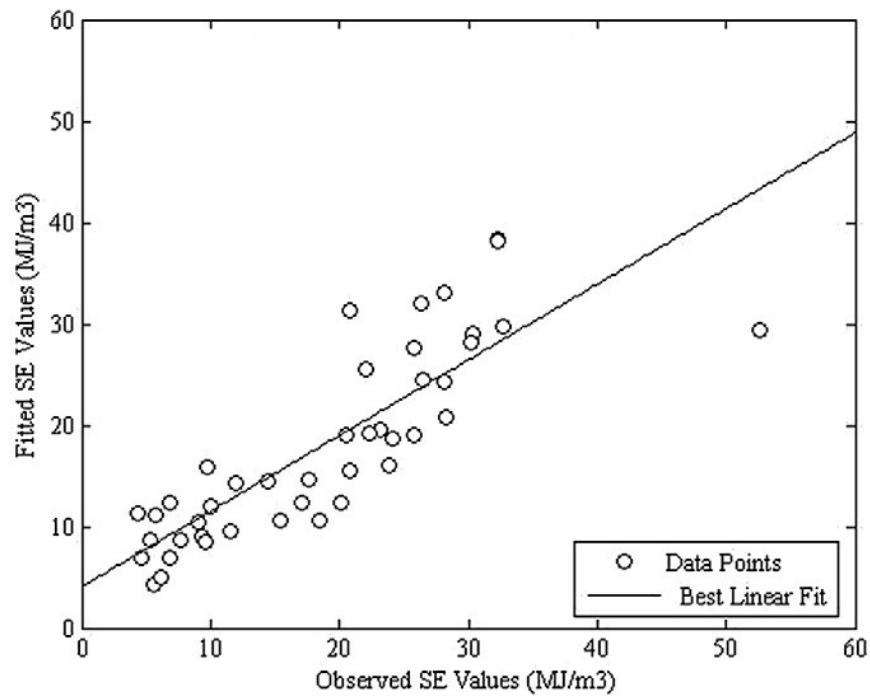Figure 25 shows the scatterplot of the observed and predicted SE.

Figure 25: Tiryaki nonlinear regression model (Tiryaki 2008)

3.3.4 Tiryaki model II

The next model of Tiryaki (2009) uses a regression tree model to estimate the SE for excavating tunnels. A regression tree can be interpreted as an if-then relationship between different layers. Tiryaki concluded, that the SE is depending on four independent variables. Those were the UCS, BTS, Elasticity and CAI.

Figure 26 presents a regression tree to estimate the SE (MJ/m³) over the modulus of elasticity (GPa) (fluctuation range: 80.6 – 5.6), the cone indenter hardness (ranges from 27.8 – 1.3) and the BTS (MPa) (ranges from 21.3 – 1).

Figure 27 shows the scatterplot between the observed and modulated SE. This estimation fits with a very good correlation coefficient of 0.97.
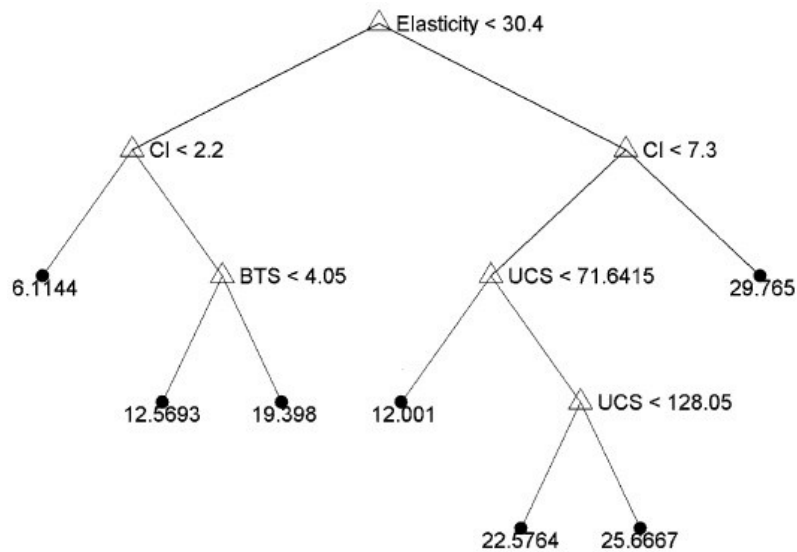
Figure 26: Regression tree for SE (Tiryaki 2009)
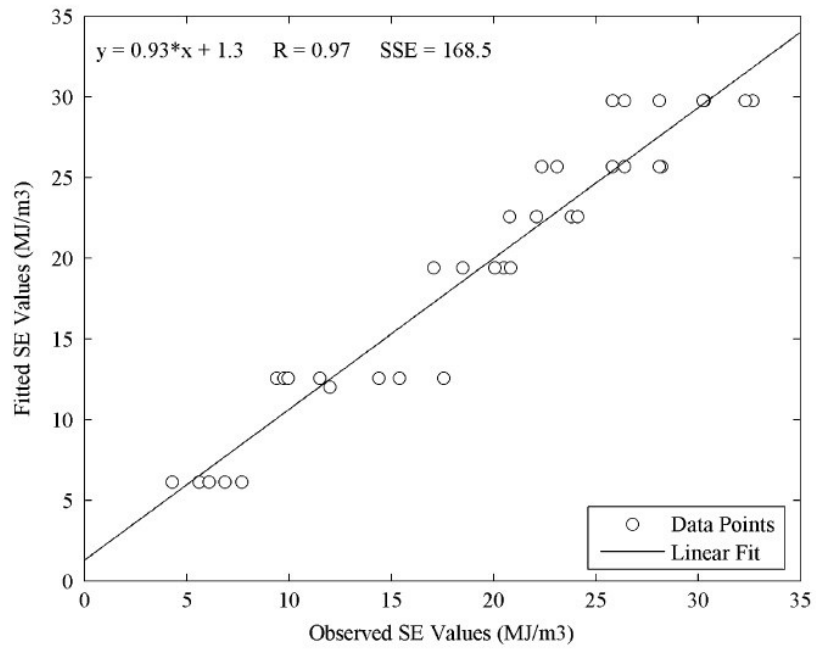
Figure 27: Modulated SE observed SE (Tiryaki 2009)

3.3.5 Tumac Bilgin model

This model was published by Tumac et al. (2007). Its target is to estimate the cuttability from two parameters (shore hardness (SH) and UCS).

They use the equation 15 to calculate the ICR using the SE.

In Figure 28 the $SE_{optimum}$, which is calculated out of laboratory tests, is presented.
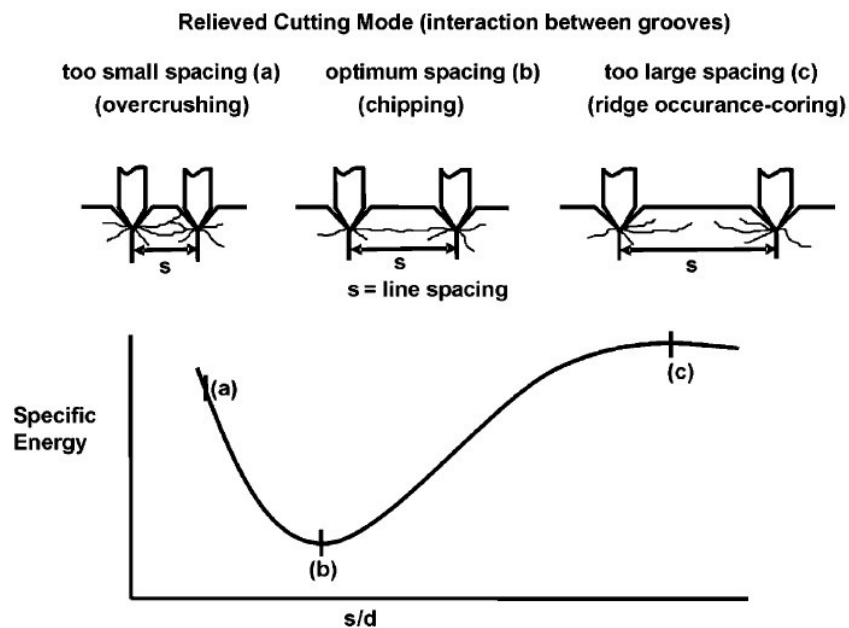
Figure 28: $SE_{optimum}$ in cutting test (Tumac et al. 2007)

In Figure 29 the correlation between the SE and SH is presented. The equations below show these mathematical correlations.

$$SE = 0.2316 * SH1 - 2.0066 \qquad (23)$$

$$SE = 0.1705 * SH2 - 3.9468 \qquad (24)$$

SH1… average of 50 points (ranges for limestone around 54)

SH2… result of 15 tests at one location (ranges for limestone around 72)

The correlation coefficient of this equations were 0.78 and 0.44.
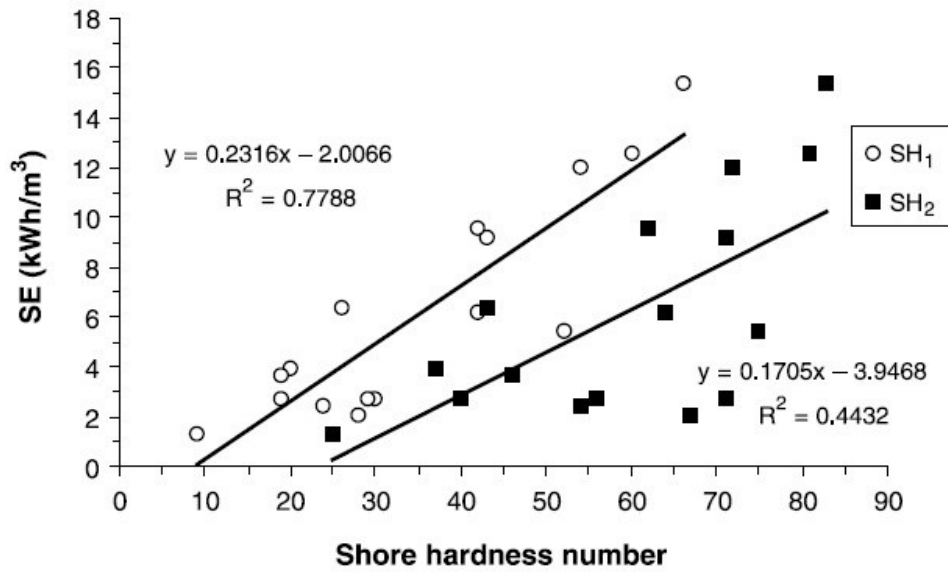
Figure 29: Relation between specific energy and shore hardness (Tumac et al. 2007)

If this data is set into the equation for NCR.
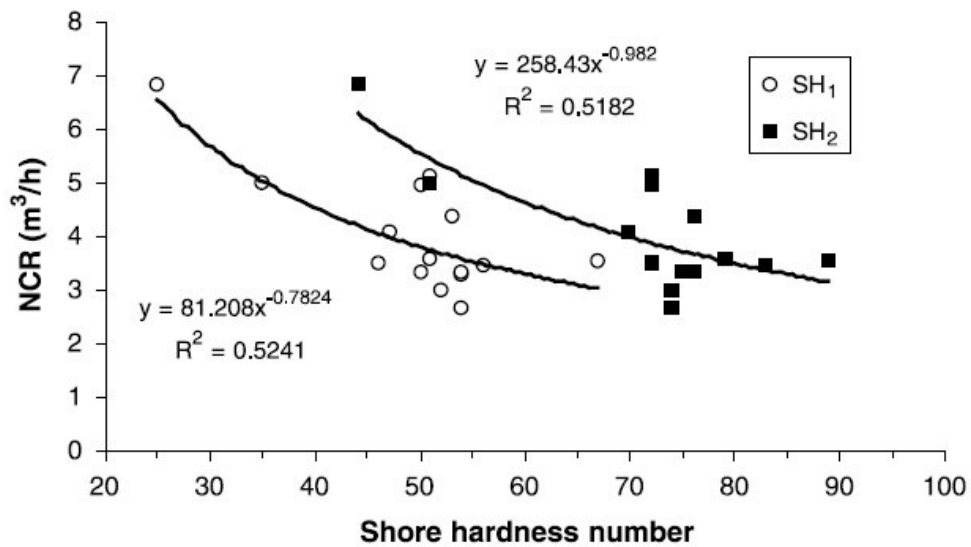
Figure 30: Relation between NCR and SH (Tumac et al. 2007)

The equations in Figure 30 show the final result of the Tumac et al. paper.

For the application in this thesis this correlation factors, SH and NCR´, will not guide to a successful performance model.

3.3.6 Yilmaz model

This model is using the hybrid dynamic hardness (HDH) to estimate the ICR of roadheaders.

The HDH is a relation between different measured rebound hardnesses. It is described by the equation below.

$$HDH = ESH_s^2 * ESH_r \qquad (25)$$

Here ESH_s stands for the surface hardness of rock established by using the hardness test (Figure 31)(ranges for limestone around 72). It gets calculated out of the average of 20 rebound tests (different spots) (ranges for limestone around 54).

And ESH_r stands for the peak hardness value, which is measured at the impact on one single spot.

Figure 31: Surface hardness tester (Yilmaz et al. 2015)

Yilmaz et al created a equation for the SE which can be seen below:

$$SE = 0.2662 * HDH + 0.1975 \qquad (26)$$

The correlation coefficient of this equation is 0.91. The equation fits for rocks with a UCS between 10 and 170 MPa.

To estimate the ICR the common equation (27) is used again.

$$ICR = k * \frac{P}{SE} \qquad (27)$$

Yilmaz et al recommended in their paper in the year 2015 that also the RQD value should be taken into consideration, otherwise the ICR will just depend on one single parameter.

3.4 Geological and geotechnical factors

Of course geological and geotechnical factors also influence the cutting performance, as well as the parameters written in the chapters above. A change of input-parameters always influences the output result.

Bilgin et at published in the year 2004 several equations including geotechnical parameters:

The specific energy:

$$SE = \frac{\sigma_c^2}{2E} \qquad (28)$$

Instantaneous cutting rate per time (also known as NCR):

$$ICR = k * \frac{P}{SE_{opt}} (29)$$

σ_c … compressive strength (MPa)   E …Young's modulus (MPa) P…cutting power (kW)

SE_{opt} …optimum specific energy (kW/m³) (see Figure 28) k …energy transfer coefficient

The energy transfer coefficient k alternates for roadheaders between 0.45 and 0.55.

Important to mention could be that utilization time can influence the excavation in a positive or negative way.

The geological factors could be:

- strata inclination /tunnel inclination

This effect is mentioned in chapter 3.1

- effect of water

Water can reduce friction and rock strength in joint systems. The ICR can reach double in performance than in dry zones (material specific).

- wet sticky zones

Sticky material (influenced by: water absorption, plastic limit and liquid limit) can reduce the ICR up to a factor of 2.5, because the cutting head can be filled with material. Figure 32 presents such a unwanted cutting head.
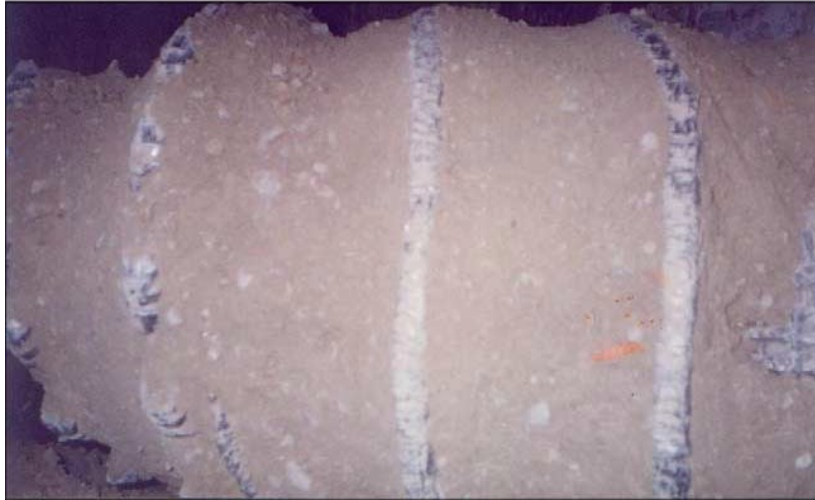
Figure 32: cutting head pollution during sticky zone (Bilgin et al. 2004)

- Effect of lamination

Bilgin et al also wrote in their paper (2004), that a lamination smaller than 100 mm increases the ICR. The spacing of joints (related to RQD-value) have the same influence to the ICR.

4 Alternative rock fragmentation technics

4.1 Water jet cutting

4.1.1 Introduction

The water jet cutting technology was invented during the 1960 years. In the case of rock cutting abrasive particles (most used: garnet, alumina, silicon carbide, glass beads) in the water beam are used.

Paul et al. published (1998), that the operating fluid pressure varies between 150 - 400 MPa, the beam width between 0.1 - 0.4 mm and the velocity of the beam varies between 200 – 800 m/s and follows the equation below.

The equation below was invented by Liu et al (2015) and calculates the beam velocity out of the water pressure:

$$v = 44.67 * \sqrt{P} \qquad (30)$$

v… beam velocity (m/s)   P… pressure

Figure 33 shows the principal design of the nozzle
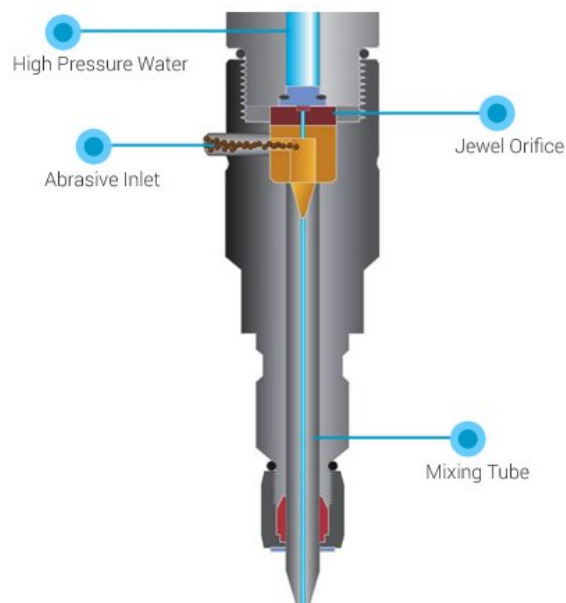
Figure 33: Water jet nozzle (www.omax.com)

4.1.2.1 Geometric influence

There are a view combinations of different geometric factors which can influence the result of water jet cutting in a direct way. These factors are:

- standoff distance effect

Oh et al wrote in their paper (2014), that a shorter standoff distance will create better fracturing results, than longer standoff distances. This result is based on the expansion of the water jet in diameter over the distance (focusing characteristics). The testing of the critical standoff distance, tested on a preconditioned sample is presented in Figure 34. The artificial holes in the center of the sample have to be 35 ± 15 mm deep and in cylindrical shape. The result for 25 mm free surface samples (sample shape 50 x 50 x 100 mm) is presented in Figure 35.
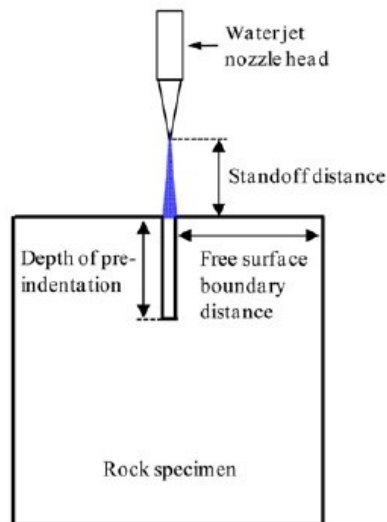
Figure 34: Water jet geometric parameters (Oh et al. 2014)
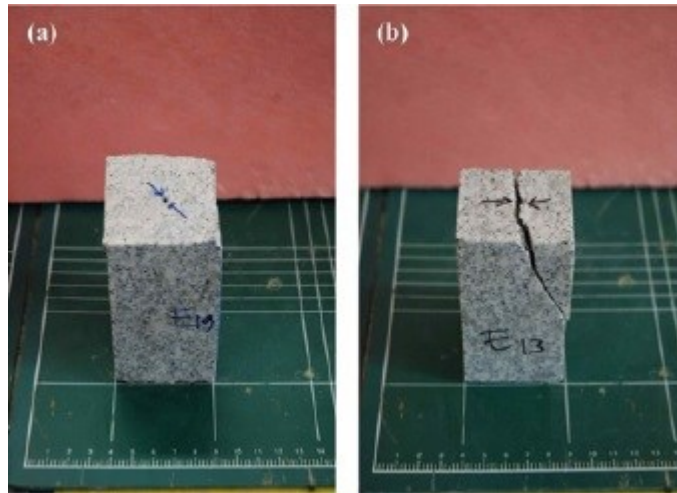
Figure 35: Effect of standoff distance on granite; distance 130mm (a), distance 10mm (b) (Oh et al. 2014)

- pre indentation effect

A pre drilled target hole greatest easier breakage conditions for longer standoff distances (of not possible to access closer). Low water flow rates may be not able to great fracturing without this target hole (also influenced by the free surface effect).

- free surface effect

The crack resistance increase with increasing distance to the free surface of the sample. If the distance is to far just conical erosion (angle approximately 75°) can be detected (no fracturing will spread to the free surface). In the study of Oh et al this critical distance was 150 mm away from the center point of the water jet (water pressure 250 MPa, flow rate 9.6 l/min).

4.1.2.2 Pure water jet compared to abrasive water jet cutting

Five independent parameters influence the efficiency of pure water jet cutting operations. Those were:

- water jet pressure (MPa)
- nozzle diameter (mm)
- standoff distance (mm)
- traverse speed (mm/min)
- angle of impact (°)

The equation below represents the relationship of the penetration depth.

$$h = A * p^{1.5} * d_0 * e^{-2.5\,(1.62*L)} * v_p^{-0.38} * \cos \propto \qquad (31)$$

A… constant   p… pressure d_0… nozzle diameter

L… standoff distance v_p… traverse speed   α… angle of impact

Gryc et al. characterized the water yet in their paper (2014) by eight parameters:

- water jet pressure (MPa)
- nozzle diameter (mm)
- size of input abrasive particles (mm)
- diameter of focusing tube (mm)
- length of focusing tube (mm)
- standoff distance (mm)
- traverse speed (mm/min)
- angle of impact (°)

The equation below represents the relations of the penetration depth h:

$$h = B * p^{1.2} * d_A^{0.9} * e^{-2.5*\,(1.15*L)} * v_p^{-1.5} * \cos \propto \qquad (32)$$

B… constant   p…pressure d_a…focusing tube diameter

Table 9 presents the comparison of this two different techniques.

Table 9: Abrasive and pure water jet results (Gryc et al. 2014)

Rock name	Depth of cut for AWJ [mm]	Depth of cut for pure WJ [mm]	C—The coefficient for transformation of results from WJ to AWJ and vice versa
Azul Noche	9.98 ± 0.94	5.28 ± 0.19	1.89 ± 0.11
Belfast	6.24 ± 0.64	2.92 ± 0.62	2.14 ± 0.25
Rosa Beta	12.00 ± 2.26	5.77 ± 0.67	2.08 ± 0.15
New Imperial	8.94 ± 0.88	4.70 ± 0.67	1.90 ± 0.09
Shiwakashi	15.53 ± 1.33	7.03 ± 1.13	2.21 ± 0.17
Juparaná Gold	14.96 ± 1.03	7.46 ± 0.93	2.01 ± 0.11
Bílina	24.75 ± 3.22	12.15 ± 1.77	2.04 ± 0.03
Godula	17.07 ± 1.55	8.42 ± 1.44	2.03 ± 0.17
Hořice	83.45 ± 7.64	36.47 ± 4.23	2.29 ± 0.06
Javorka	48.57 ± 4.48	20.42 ± 4.24	2.38 ± 0.29
Řeka	21.52 ± 2.45	11.13 ± 1.41	1.93 ± 0.02

The coefficient C is the multiplier (average factor 2) to compare pure water jet and abrasive water jet cutting depths to each other.

The interpretation of this results will be a priority use of abrasive water jets to pure water jets. The 2-times higher power will lead to a higher cutting performance.

4.2 Laser mining

4.2.1 Introduction

The targets of Laser Mining are (after Graves and O'Brien, 1998):

- Change rock parameters

- increase drilling progress

- Decrease rig time

- Automatized drilling

- Borehole stability

- cost efficiency

One of the biggest advantages of fiber lasers are the wall plug efficiency (ratio electric power to optical power) of 20%. Another advantage will be that 50.000 hours of operation time are possible without any service. The footprint of a 5.34 kW Ytterbium fiber laser is just about 0.5 m².

A typical Nd:YAG laser will need 200 kW electric power to send out 4 kW of optical power, the fiber laser will just need 25 kW of electric input-power.

The efficiency of a laser beam is further influenced by the power source (radiation force), beam width, pulse frequency, water contend of rock and residence time (pulsed or unpulsed operation mode).

4.2.2 Design of laser

There are several kinds of lasers which can be used in laser mining (after Graves and O'Brien 1998):

- fiber laser

- hydrogen fluoride (HF) and feuterium fluoride (DF) lasers λ = 2.6 to 4.2 µm

- chemical oxygen iodine laser (COIL) λ = 1,315 µm

- CO_2 laser λ = 10.6 µm

- CO laser λ = 5 to 6 µm

- free electron laser (FEL) (any wavelength possible). For Graves and O'Brien this laser is the best high-power laser for the future.

- Neodymium/Yttrium Aluminum/Garnet Laser (Nd/YAG) λ = 1.06 µm

4.2.3 Process during cutting/drilling

To increase the drilling progress, it is necessary to use the right power and the correct wavelength for each kind of rock, also the correct time of penetration will be an important factor.

Those combined-settings create some mechanical stress (change in the void space) (Graves et al., 2002).

The rock parameters: Young´s modulus, shear modulus, bulk modulus were reduced. The parameters permeability and porosity were enhanced.

In case of a high water contend, the laser induces temperature dehydrate the void space. Therefore the vapor creates (Figure 36) more cracks inside the rock (for example shale mineral).

(a) before   (b) after
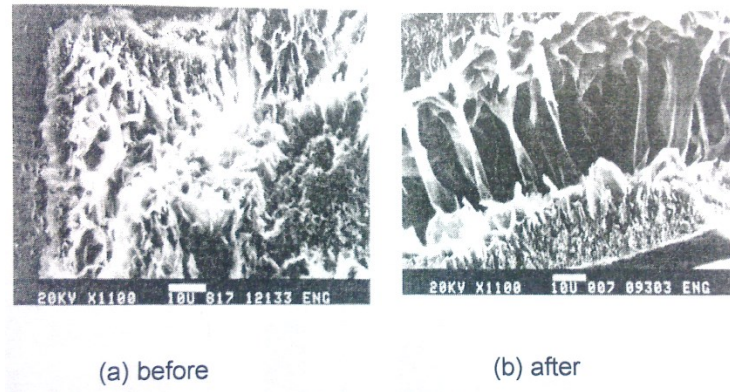
Figure 36: Dehydration of clay minerals (Graves et al., 2002)

4.2.4 Application in rock cutting

Ahmadi et al. described in their paper in the year 2011 the specific energy of an Nd:YAG laser with the equations below.

$$SE = \frac{E_i}{V_r} \qquad (33)$$

$$E_i = t * W \qquad (34)$$

$$ROP = \frac{D}{t} \qquad (35)$$

E_i…input Energy (J) V_r…removed volume of rock (cm³)   t… duration of laser beam (sec) W…average laser power (watt)   D…Depth (mm)   ROP…rate of penetration (mm/s)

After several experiments with different time intervals and dry or saturated samples they invented a equation for the average required power (watt). This equation can be seen below:

$$P_{ave} = 0.262 * SE * ROP * D^2 \qquad (36)$$

D…diameter of hole (mm)   SE…specific energy (kJ/cm³)   ROP…rate   of penetration (mm/s)
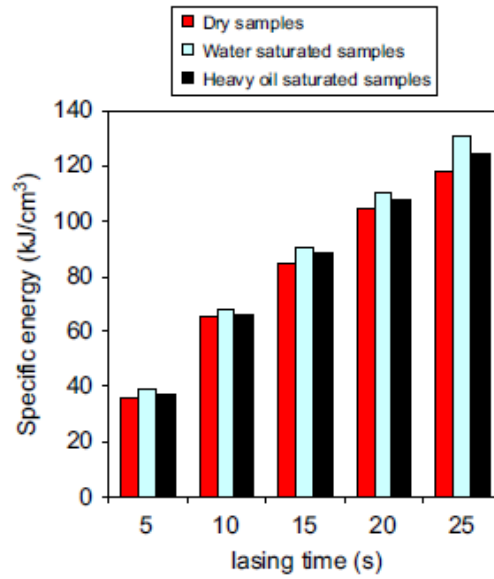
Figure 37: Specific energy (Ahmadi et al. ,2011)

Out of their investigations on limestone the equation below can be made:

"Duration: 25 sec

Typ:TLD-5 (Dry)

Depth of hole: 11.58 mm

Specific energy: 117.76kJ/cm³"

$$SE_{laser\ 100mm/50mm} = \frac{117.76\ kJ/cm^3}{11.58\ mm} * depth_{\frac{100mm}{50mm}} * \frac{30sec}{25sec} \qquad (37)$$

Out of figure Figure 37, the SE for limestone after 30 sec of irradiation (using a laser density of 30.3 kW/cm²) of about 1220 (kJ/cm³) for 10 cm penetration and 610 for 5 cm can be calculated.

4.3 Microwave fragmentation

4.3.1 Introduction

Each wave is defined by their wavelength and amplitude. The microwaves are classified as electromagnetic waves with a frequency between 300 MHz and 300 GHz. Related to the equation below the result of the wavelength varies between 1 m and 1 mm (10^{-3} m) (after Toifl 2016). Other characteristic waves can be seen in Figure 38.

$$c = f \times \lambda_0 \quad (38)$$

c… propagation speed (in vacuum 300.000 m/s)   f… frequency of wave (Hz)
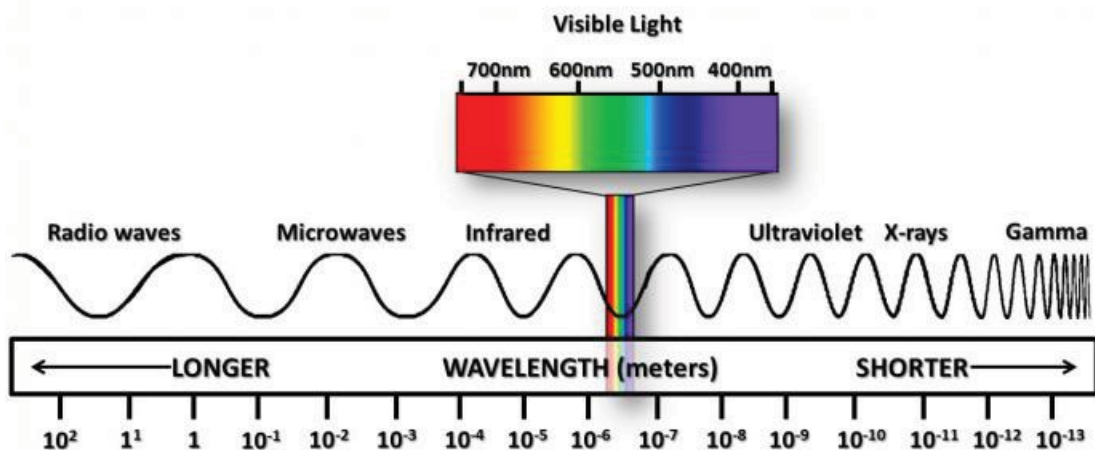
λ_0… wavelength (m)

Figure 38: Wavelengths of different wave kinds (Toifl 2016)

4.3.2 Physical heating with microwaves

Each wave which interacts with a medium (in our case the rock) obeying to the following mechanisms:

- reflection
- transition
- absorption

To heat up a medium a high grade of absorption of the electromagnetic energy has to be reached. The other mechanism heat the medium slower than the absorption effect.

To successful emit microwaves three hardware-components are necessary. Figure 39 below is presenting this in a very rough way:
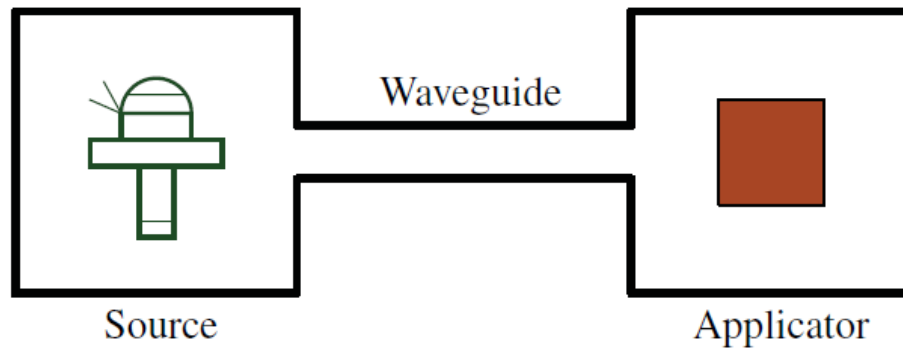
Figure 39: Equipment of microwave production (Toifl 2016)

The sources can be:

- Magnetons

- Klytrons

- traveling wave thermionic devices

- Gyrotrons

- Magnicons

- Ubitrons

- Peniotrons

For the applicator two different technics are suitable:

- Multimode cavities (use in the household oven)

- Single mode cavities (may use in rock heating applications)

5   Alternative RMR / RMR and cutting
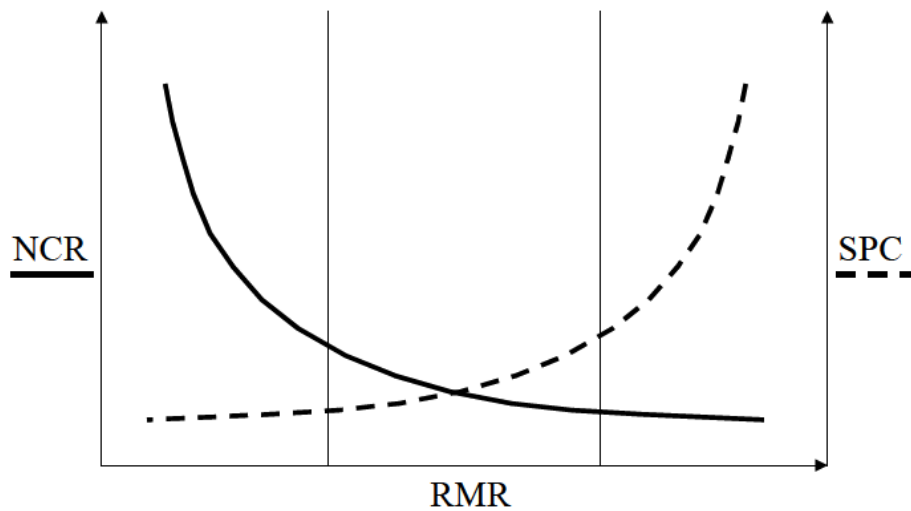
Figure 40: Goal of preconditioning (Restner and Gehring 2000)

Roadheaders are widely used in mining and tunneling for quick and flexible excavations. Their performance is limited by several parameters (see chapter 3). Alternative fragmentation methods try to reduce those parameters by introducing artificial cracks in order to increase the performance of these machines.

The goal of this thesis is to review existing performance prediction models (see chapter 3) in this context. Several theoretical scenarios have been developed in this chapter of how the best "pre damage/conditioning" model has to look like in order to assist the conventional method. As can be seen in Figure 40 the influence of RMR (spacing, …) on the NCR/ICR is contrary.

As efficient those preconditioning (loss of internal rock mass strength) of the face will be, the higher the hybrid cutting performance will be.

The influence of abs. RMR on hybrid ICR is shown in the upper part of Figure 41. The influence of rel. RMR to rel. ICR and the consequential microwave antenna spacing is shown in the lower part of Figure 41 (was made for limestone with a start abs. RMR of 81).

This results shows the same trend stone predicted by Restner and Gehring.
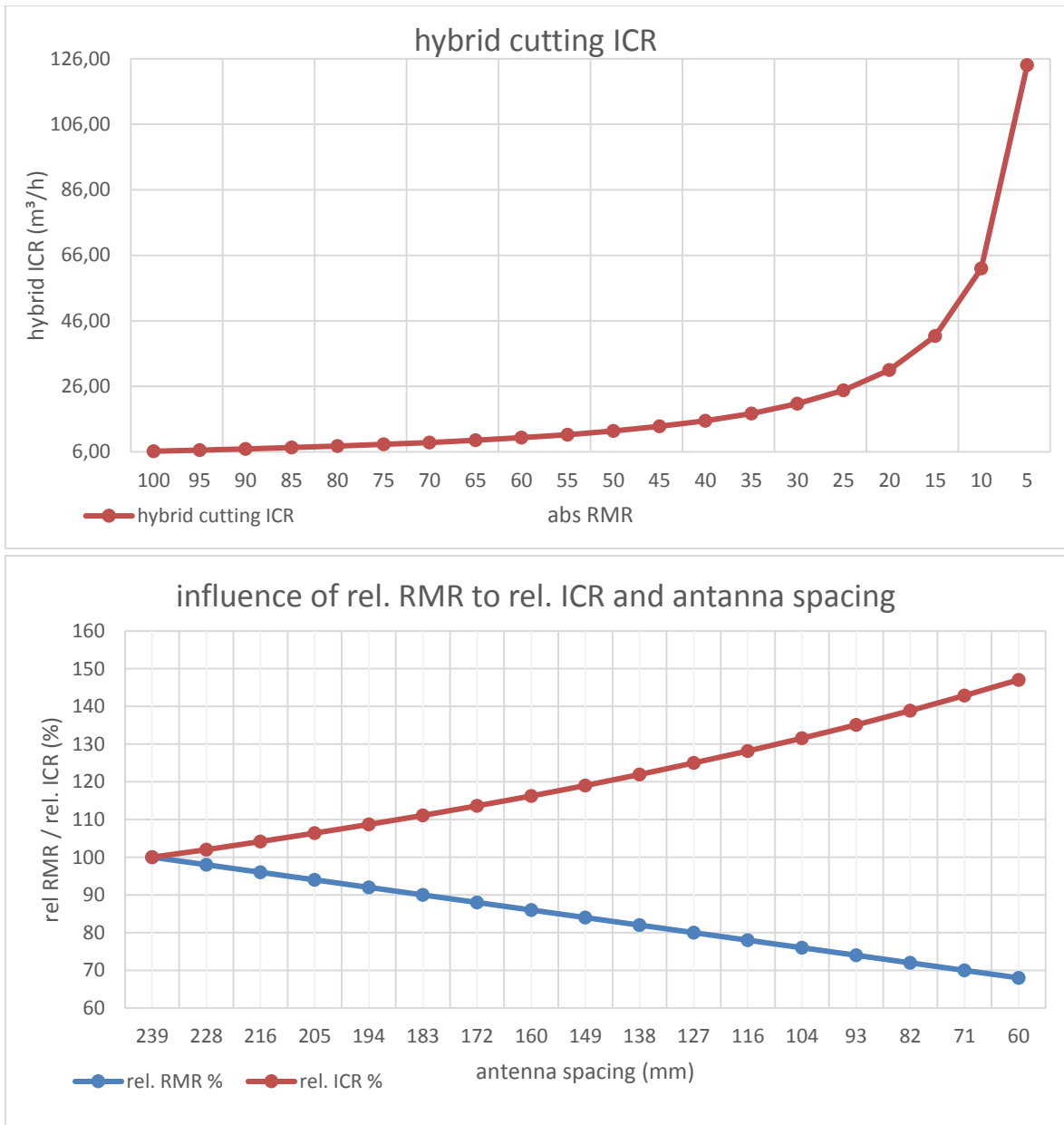
Figure 41: Influence of rel. RMR to rel. ICR and antenna spacing

For the following theoretical forecast, a time slot of 10 seconds of residence time was chosen. During this time the alternative fragmentation methods have to damage the rock at their best behavior. After 10 seconds the pick will excavate the weakened rock mass to a total depth of 100 mm. The chosen rock type in this forecast is limestone, its geotechnical properties are shown in Table 10. Limestone was chosen, because of its well-known parameters and the assessable cutting performances.

Table 10: Rock properties of limestone used in the study

		lower range	upper range	chosen value
Ultrasonic velocity (Vp)	m/s	3500	6000	4750
Porosity (n)	%	15		15
UCS	MPA	75	250	150
BTS	MPA	14	35.7	24.85
CAI		0.5	1	0.75
Rn		30	37	33.5
Density (dry)	g/cm³	2.3	2.7	2.5

The cutting depths for UCS in the range between 75 - 150 MPa is set to 10 cm.

For UCS in the range between 150 - 250 MPa the cutting depth is set to 5 cm.

The installed cutting power of the roadheader is 300 kW.

In a second stage the forecast models (chapter 3.3) will be set into relation of different rRMR values.

5.1 Influence of RMR on ICR

A lower rock mass classification means an easier/lighter access of the pick into the rock mass. If this idea will think forward the tunnel face can be excavated with a higher speed, than without preconditioning. Best situation of preconditioning will mean the same depth as the typical cutting depth (normally half of roadheader-drum size).

For the theoretical forecast a linear regression between the original ICR and the hybrid cutting ICR has been supposed. If the spacing will get closer the hybrid ICR, because of its contrary relation, will get higher. The equation below shows these relation:

$$ICR_{hybrid} = \frac{ICR_{original}}{\left(\frac{rRMR}{100}\right)} \qquad (39)$$

$ICR_{original}$… value out of mechanical model (chapter 3)

$rRMR$… Rock mass rating after preconditioning

As a general statement can be recorded, that all models were made for site specific forecast situations. A short discussion of the advantages and disadvantages of them can be found at the next page.

5.1.1 Ocak & Bilgin model

The first model (axial) correlates, with just the variable (UCS, RQD, P), in the upper ranges of UCS good to the performances of in situ excavations. But it is not the best correlation in this paper. The original ICR ranges from 16 m³/h to 0.4 m³/h.

The second model (transversal) fits not accurate enough to the in situ performances.

5.1.2 Comakli model

For the theoretical forecast of the ICR the model of Comakli shows, with its multiple regression of all necessary parameters, the best correlation to in situ excavation performances. The original ICR ranges from 9.5 m³/h to 3.4 m³/h.

For the thesis this model was chosen. All the others can be found in the annex.

5.1.3 Tiryaki model I

The high influence of the Cerchar abrasiveness and the low influence of the UCS creates a much to high SE and ICR. The original ICR ranges from 43 m³/h to 32 m³/h.

5.1.4 Bilgin model 2004

The potential influence of UCS to the specific energy and the thus influenced cutting performance ranges (for the chosen limestone) in an abnormal high range (highest of all investigated models). The original ICR ranges from 288 m³/h to 25 m³/h.

5.2 Used technologies for preconditioning

5.2.1 Water jet and pick

Liu S. et al. described the hybrid cutting process with three steps:

- Hydraulic erosion
- Hydraulic fracturing in micro cracks
- Expansion in reaction of high pore water pressure

The authors investigated four different situations.

In Figure 42 below those techniques were presented:
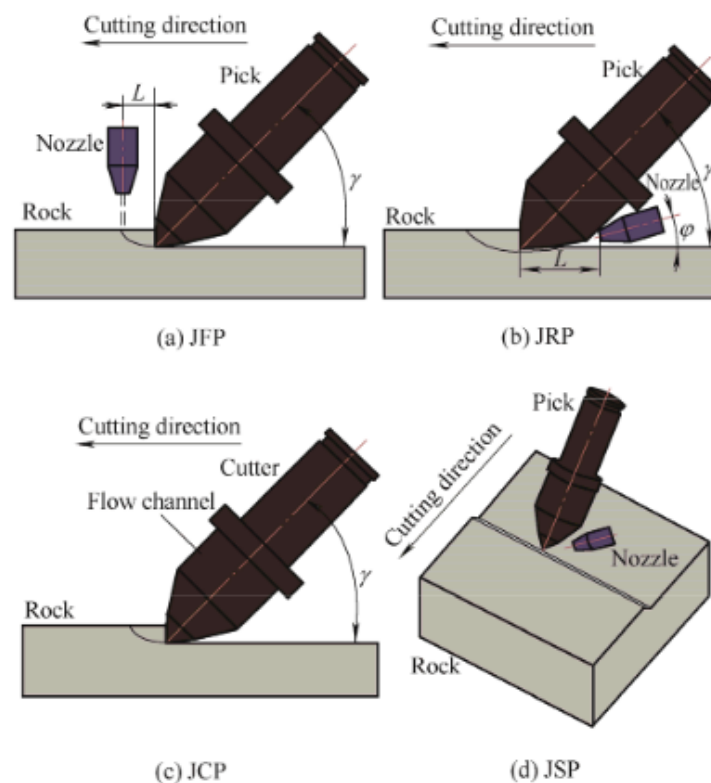
Figure 42: Water jet and pick cutting situations (Liu. et al. 2015)

Liu et al run several experiments to investigate the decreasing of the pick cutting force.

The result of their measurements are shown in chapter 6.1.

5.2.2 Laser and pick

Assumed parameter is that the laser beam creates only a vertical hole and no further cracks were induced into the rock mass.

The figure below (Figure 43) should demonstrate two possible designs for preconditioning the rock mass within the 10 seconds of residence time. A line cutting (crosscutting) with laser will not be possible within the time window of 10 seconds.

Option A were parallel drilled holes in a regular pattern. A very rough surface after extraction with the pick could be expected, because the pick will shear the rock off along those lines. If the holes are in one line to each other the next off-center pick will have a higher resistance than the center pick.

Option B should prevent such a rough surface with an irregular and inclining (45°) laser pattern. The influence of spacing to depth ration (s/d) can be seen in Figure 28.

Table 11 shows the RMR rating of the original limestone face and the rating after preconditioning (estimations). The small table left and right show the detail of "condition of discontinuities" for the two different cutting depths.

The power for each laser beam 7.7 kW for a cutting depth of 10 cm and 1.9kW for 5 cm is calculated.

As result, for the preconditioned area (0.5 m x 1 m) 78 holes are necessary to reach the desired rRMRs. The total laser power reaches 600 kW for 10 cm and 150 kW for 5 cm cutting depth.
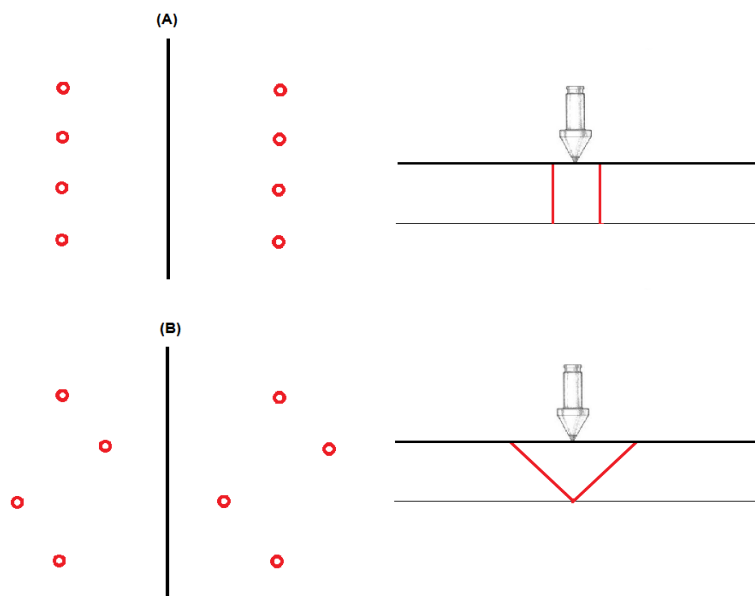
Figure 43: Laser induced damage

Table 11: RMR for laser preconditioning

	Bieniawski RMR				10 cm cutting depth		5 cm cutting depth	
	original				after preconditioning (rRMR)		after preconditioning (rRMR)	
Factor	lower	upper	%			%		%
Strength of rock	12	12			12		12	
RQD	13	17			13		11	
Spacing	10	10			8		8	
Condition of discontinuities	30	30			22*		17**	
Groundwater	0	0			0		0	
sum	65	69	100		55	82.09	48	73.64
average	67							

*Detail of: Condition of discontinuities	10 cm cutting depth
discontinuity length	6
separation	0
roughness	4
infilling	6
weathering	6
Sum	22

**Detail of: Condition of discontinuities	5cm cutting depth
discontinuity length	4
separation	0
roughness	1
infilling	6
weathering	6
Sum	17

5.2.3 Microwave and pick

The assumed parameter of microwaves is that the preconditioning voided cracks with vertical extension (no horizontal cracks).

The cracks will change the excavation process into an easier rip situation for the rock pick.

As a result, the hybrid ICR of microwave preconditioned rock will be higher than the hybrid cutting ICR of laser preconditioned applications. Another advantage could be, that the face will not get as hot as laser treated rock (prevent thermal pick wear).

In Table 12 the influence of various microwave irradiation problems on the RMR is presented.

Figure 44 below shows a possible layout of the microwave antennas and the associated damage pattern.
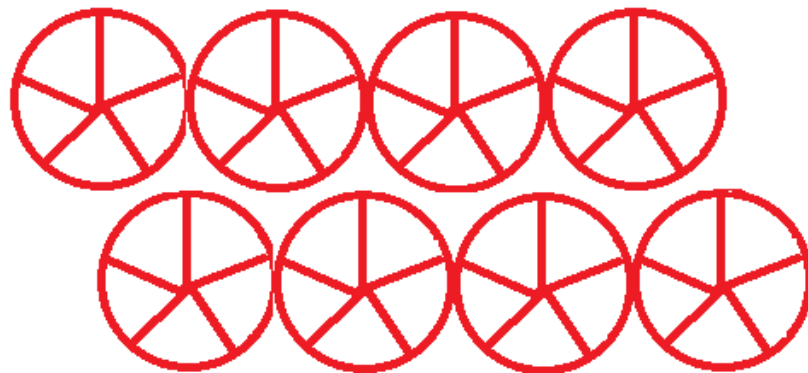
Figure 44: Sequence of microwave antennas

Table 12: RMR for microwave preconditioning

Bieniawski RMR				10 cm cutting depth				5 cm cutting depth			
	original			after preconditioning (rRMR)				after preconditioning (rRMR)			
factor	lower	upper	%		%				%		
Strength of rock	12	12		12				12			
RQD	13	17		13				10.5			
Spacing	10	10		8				8			
Condition of discontinuities	30	30		22*				20**			
Groundwater	0	0		0				0			
sum	65	69	100	55	80.60			50.5	75.37		
average	67										

*Detail of Condition of discontinuities	10 cm cutting depth
discontinuty length	5
seperation	0
roughness	4
infilling	6
weathering	6
sum	22

**Detail of: Condition of discontinuities	5 cm cutting depth
discontinuty length	4
seperation	0
roughness	2
infilling	6
weathering	8
sum	20

6 Theoretical influence of preconditioning technologies

6.1 Influence of water jet cutting

The results of water jet adjust cutting are presented in Figure 45 below.
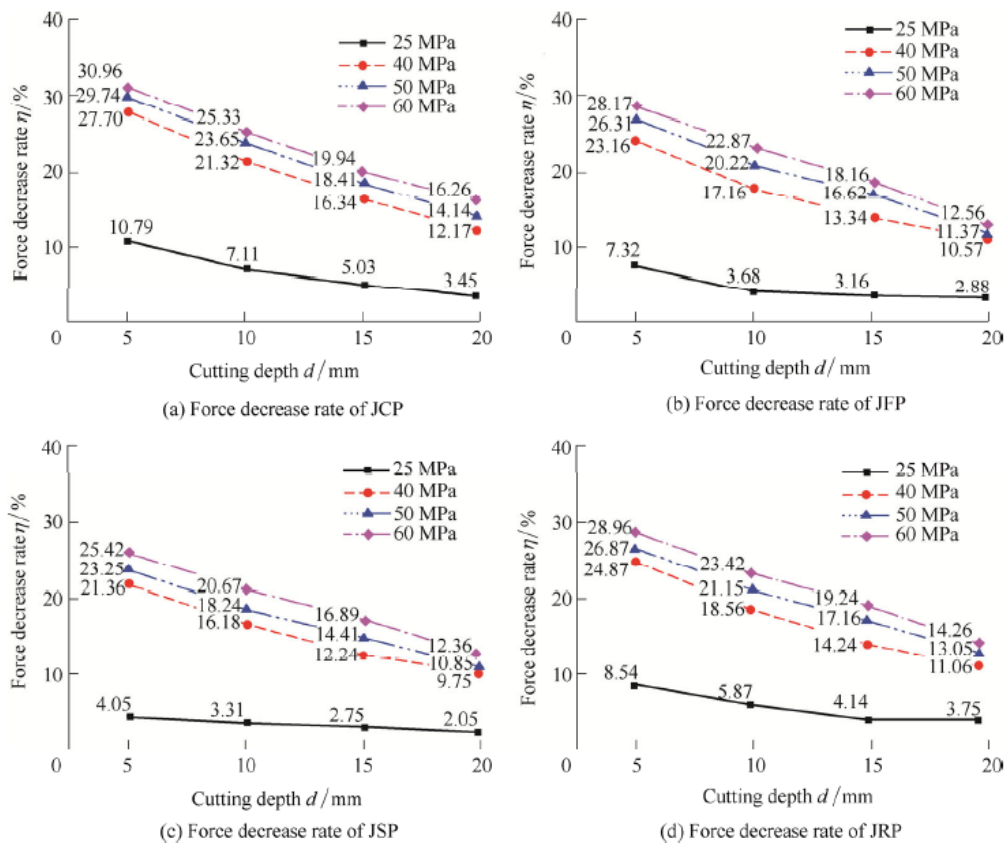
Figure 45: Pick force reduction by water jet (Liu S. et al. 2015)

As a special result for JSP an optimum distance between the nozzle and the pick tip of 2 – 5 mm was noticed. For the distance larger than 5 mm the water jet creates its own damage zone beside the zone of the pick. This situation is presented in Figure 46.
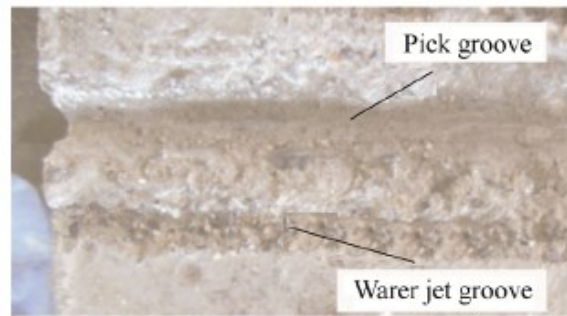
Figure 46: Non optimum distance for JSP (Liu S. et al, 2015)

As result for this thesis, the version JSP will not guide to the best improvement in hybrid cutting with water jet and pic. The first choice would be version JCP.

6.2 Influence of laser cutting

6.2.1 Comakli model

The model of Comakli shows the most realistic cutting performance of all the prediction models. The model specific equation (20) was used to calculate the SE out of the input parameters. Equation 15 was used to calculate the original ICR out of the specific energy. And equation 39 was used to calculate the hybrid cutting ICR out of the original ICR.

Table 13: Laser hybrid cutting model Comakli

UCS	SE	Original ICR	hybrid cutting ICR
75	12.58	9.53	11.60
100	19.18	7.55	9.20
125	25.78	6.25	7.61
150	32.38	5.33	6.50
175	38.98	4.65	6.49
200	45.58	4.12	5.76
225	52.18	3.70	5.17
250	58.78	3.36	4.69

Depending on a different cutting depth and preconditioning situation a difference between 21.8 % and 39.5 % of the ICR could be achieved.
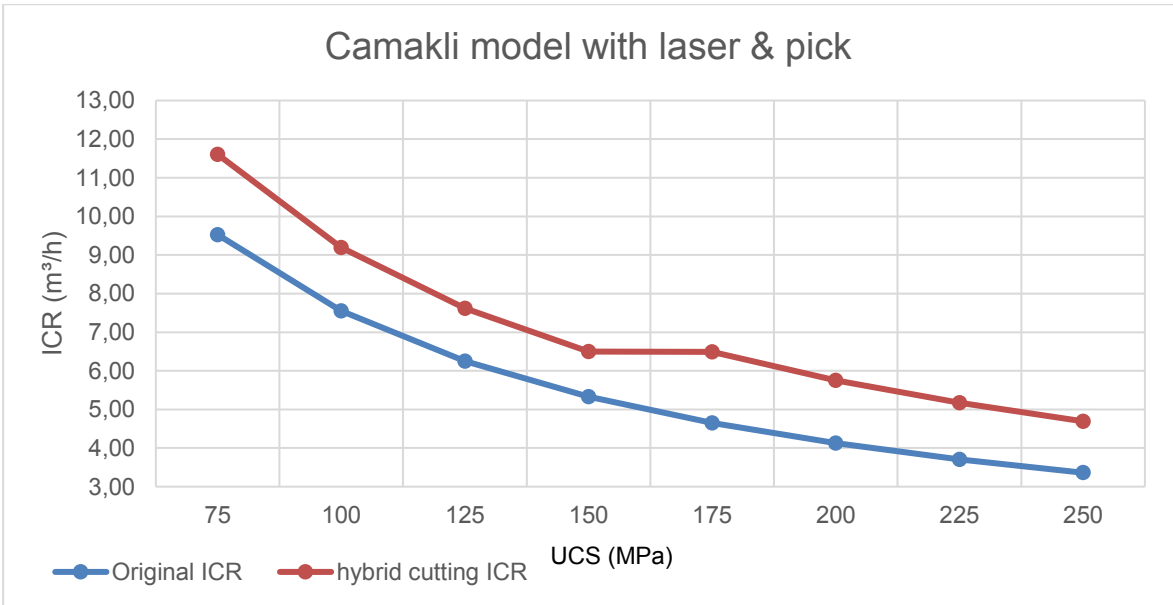
Figure 47: Hybrid cutting Comakli model (laser)

The remaining models of Tiryaki (I+II) and Yilmaz produce not realistic results (with use of standard limestone specific parameters) and were not shown in this thesis.

6.2.2 Laser rRMR Comakli model

Table 14 below shows how a different rock mass rating influence the hybrid cutting performance:

Table 14: rRMR Comakli model (laser)

abs RMR	rel. RMR	original SE	original ICR	hybrid cutting ICR
82	100	38.69	6.20	6.20
80	98	38.69	6.20	6.33
79	96	38.69	6.20	6.46
77	94	38.69	6.20	6.60
76	92	38.69	6.20	6.74
74	90	38.69	6.20	6.89
72	88	38.69	6.20	7.05
71	86	38.69	6.20	7.21
69	84	38.69	6.20	7.38
67	82	38.69	6.20	7.56
66	80	38.69	6.20	7.75
64	78	38.69	6.20	7.95
62	76	38.69	6.20	8.16
61	74	38.69	6.20	8.38
59	72	38.69	6.20	8.62

For an easier understanding, the diagram below (see Figure 48) shows the relation of preconditioned face represented by rRMR to the hybrid cutting ICR. Equation 39 was used to calculate the hybrid cutting ICR out of the original ICR.

The difference between Table 13 and Table 14 is that Table 13 calculates with a static RMR in comparison to the dynamic RMR change in Table 14.

The rRMR could create a higher cutting performance of up to 2.42 m³/h
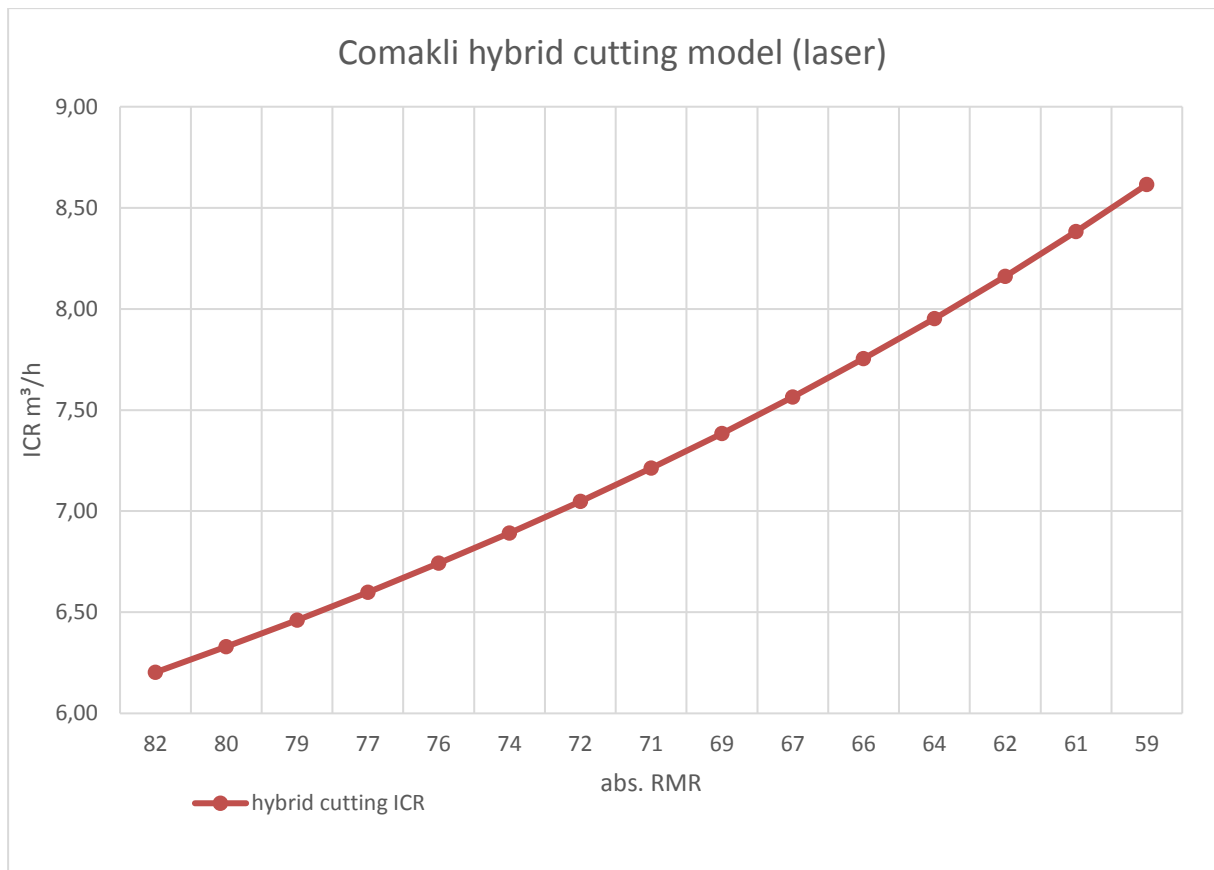
Figure 48: Hybrid cutting laser model Comakli: Influence of abs. RMR t hybrid ICR

6.3 Influence of microwave preconditioning

6.3.1 Comakli Model

The model specific equation (20) was used to calculate the SE out of the input parameters. Equation 15 was used to calculate the original ICR out of the specific energy. And equation 39 was used to calculate the hybrid cutting ICR out of the original ICR.

Table 15: Microwave hybrid cutting Comakli

UCS	SE	Original ICR	hyprid cutting ICR
75	25.20	9.53	11.82
100	31.80	7.55	9.37
125	38.40	6.25	7.76
150	45.00	5.33	6.62
175	51.60	4.65	6.36
200	58.20	4.12	5.64
250	71.40	3.36	4.60

Depending on a different cutting depth and preconditioning situation a difference between 21.4 % and 36.7 % of the ICR could be achieved.
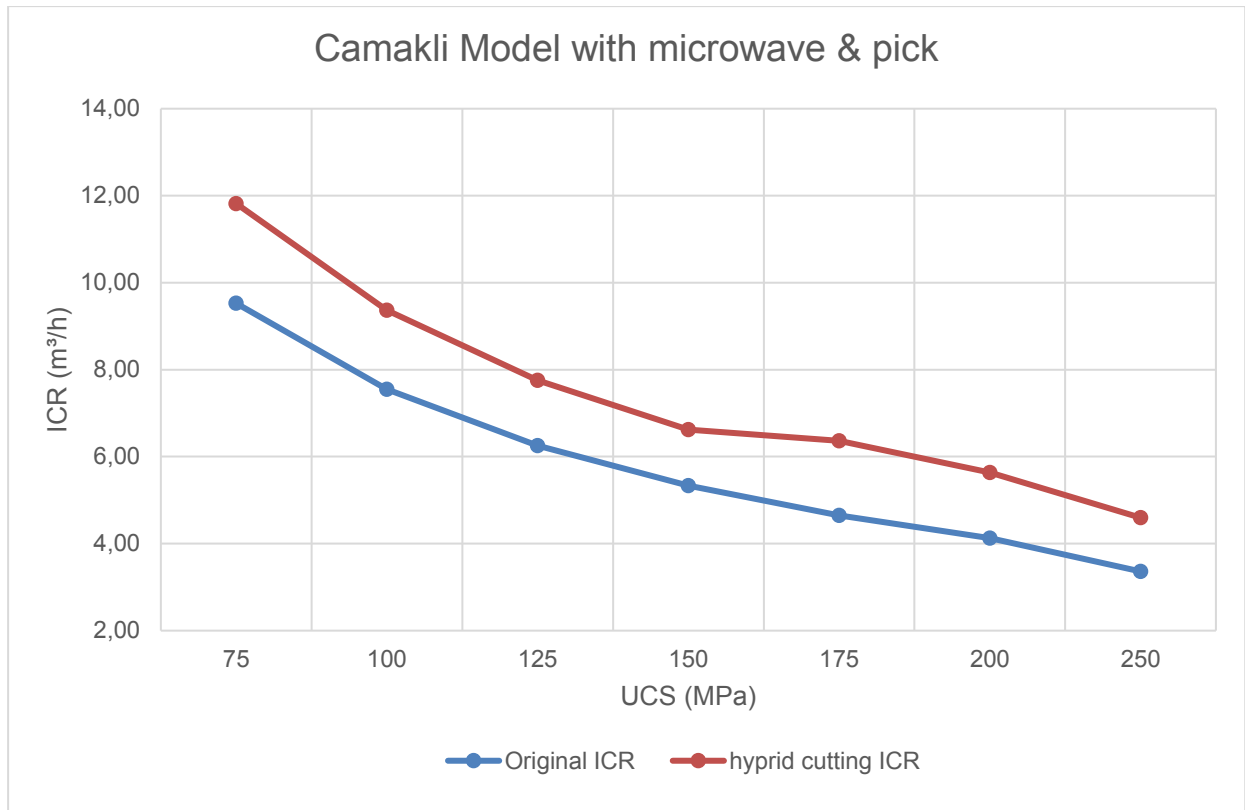
Figure 49: Hybrid cutting Comakli model (microwave)

6.3.2 Microwave rRMR Comakli

Table 16Table 14 below shows how a different rock mass rating influence the hybrid cutting performance:

Table 16: rRMR Comakli (microwave)

absoluter RMR	rel. RMR	original SE	original ICR	hybrid cutting ICR
81	100	38.69	6.203	6.20
79	98	38.69	6.203	6.33
77	96	38.69	6.203	6.46
76	94	38.69	6.203	6.60
74	92	38.69	6.203	6.74
73	90	38.69	6.203	6.89
71	88	38.69	6.203	7.05
69	86	38.69	6.203	7.21
68	84	38.69	6.203	7.38
66	82	38.69	6.203	7.56
64	80	38.69	6.203	7.75
63	78	38.69	6.203	7.95
61	76	38.69	6.203	8.16
60	74	38.69	6.203	8.38
58	72	38.69	6.203	8.62
56	70	38.69	6.203	8.86
55	68	38.69	6.203	9.12

For a better understanding. the diagram below (Figure 50) shows the relation of preconditioned face represented by rRMR to the hybrid cutting ICR. Equation 39 was used again to calculate the hybrid cutting ICR out of the original ICR.

The rRMR could create a higher cutting performance of up to 2.42 m³/h.
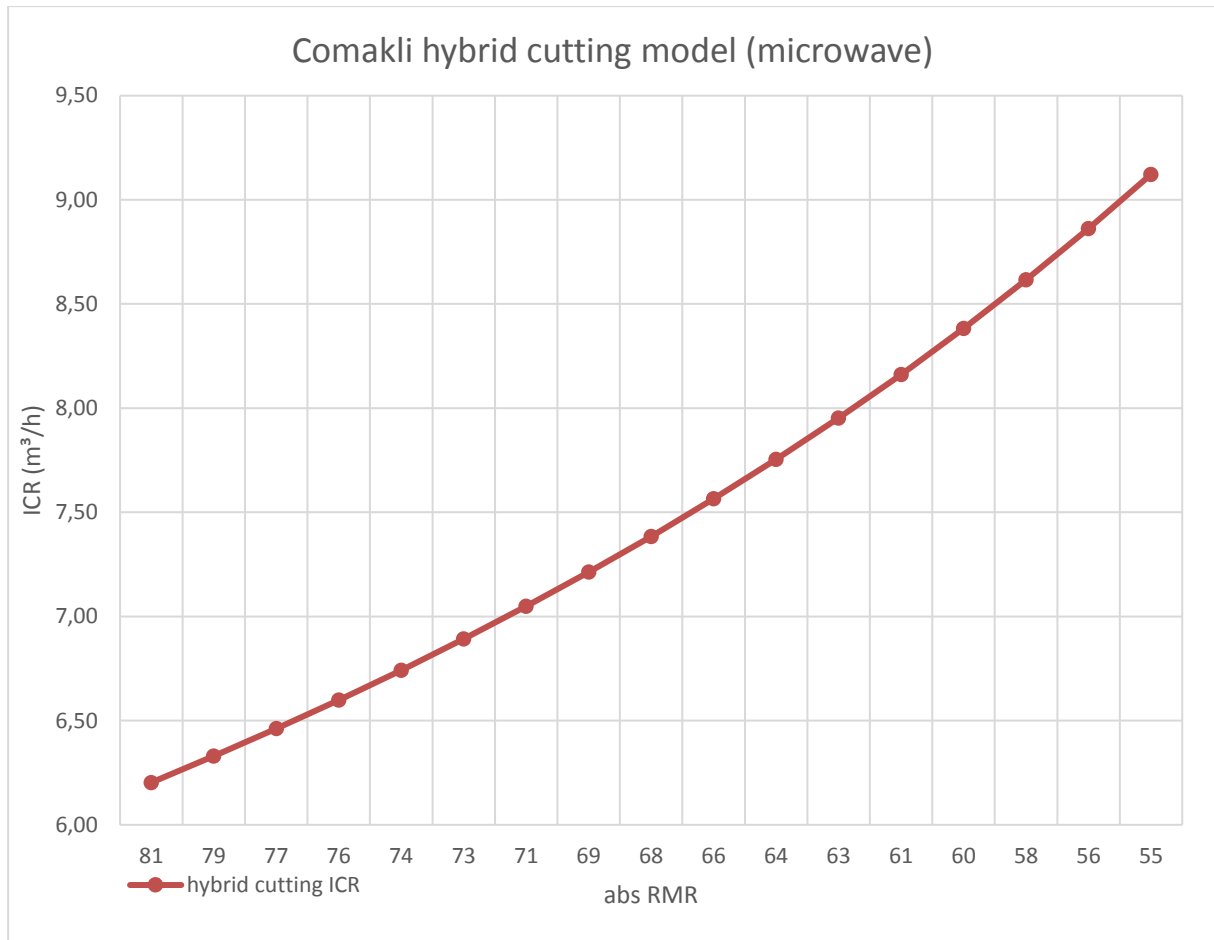
Figure 50: Hybrid cutting microwave model Comakli: Influence of abs. RMR to hybrid ICR

6.3.3 Distance between microwave antennas

As last topic in this thesis the relation between RMR and the distance between the microwave antennas is investigated.

First step was to set the absolute range of the RMR into small steps down (start see Table 12) to an arbitrary end. The relative RMR presents the percentage ration of the absolute RMR to the absolute RMR of the initial value.

Second step was to calculate the factor spacing in consideration to the relative RMR (start value see Table 12 factor 3).

Each factor spacing can be transferred into an absolute joint spacing value (here between the values 200 mm and 50 mm) (see Table 5).

Equation 40 uses the relation of arc length to radius to calculate the absolute spacing.

$$SP_{mm} = \frac{SP_{rmr}*360}{2*\pi*\alpha} \qquad (40)$$

SP$_{rmr}$… spacing out of RMR Rating   α… angle between cracks (72°)

The overlap of each antenna radius is supposed to be 25% and results in the distance between the antennas. Equation 41 shows this relation:

$$SP_{antennas} = 2 * SP_{mm} * 0.75 \qquad (41)$$

Figure 51 demonstrate the relation of absolute RMR to SP$_{antennas}$ in a graphic way.

From Table 17 it is seen, that on increase of ICR by 19% can be achieved by reducing the joint spacing from 200 mm to 125 mm. This translates to a necessary antenna spacing of 149 mm.

absolute RMR	rel. RMR	factor spacing	spacing SP_{rmr} (mm)	spacing SP_{mm} (mm)	distance between antennas (mm)	original ICR (m³/h)	hybrid cutting ICR	rel ICR %
82	100	8.0	200	159	239		6,20	100
80	98	7.8	191	152	228		6,33	102
79	96	7.7	181	144	216		6,46	104
77	94	7.5	172	137	205		6,60	106
76	92	7.4	163	129	194		6,74	109
74	90	7.2	153	122	183		6,89	111
72	88	7.0	144	114	172		7,05	114
71	86	6.9	134	107	160		7,21	116
69	84	6.7	125	99	149	6,20	7,38	119
67	82	6.6	116	92	138		7,56	122
66	80	6.4	106	85	127		7,75	125
64	78	6.2	97	77	116		7,95	128
62	76	6.1	88	70	104		8,16	132
61	74	5.9	78	62	93		8,38	135
59	72	5.8	69	55	82		8,62	139
57	70	5.6	59	47	71		8,86	143
56	68	5.4	50	40	60		9,12	147
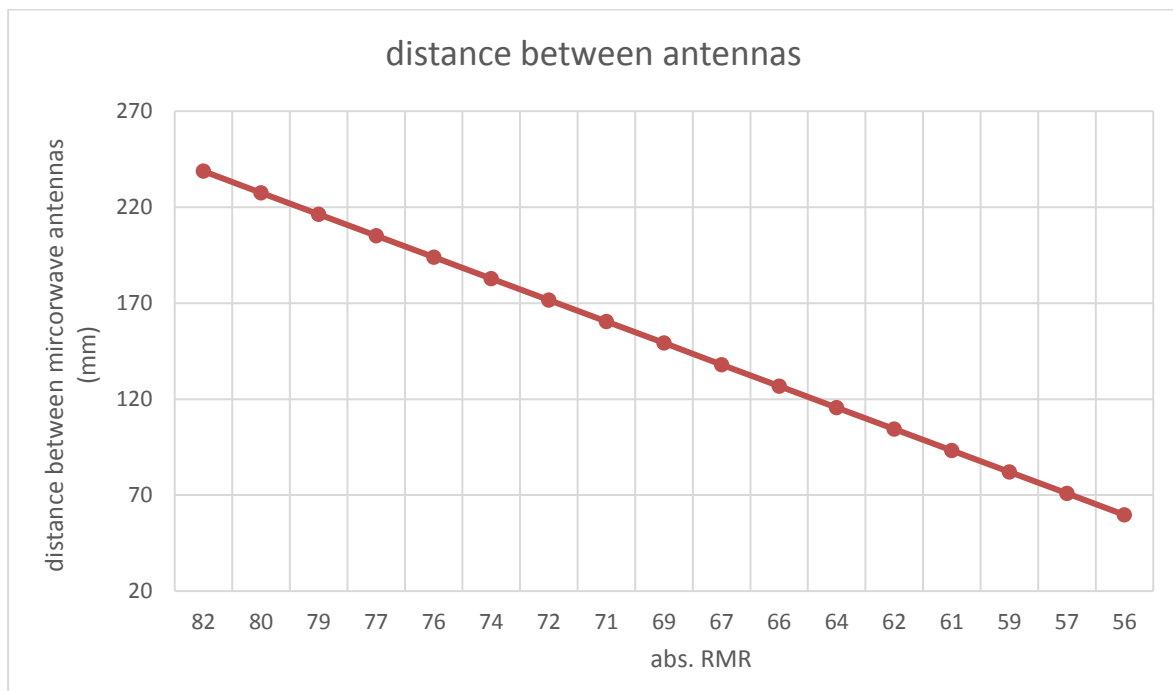
Figure 51: Influence distance between microwave antennas on abs. RMR

7 Outlook

The effect of preconditioning influences the hybrid cutting performance in the excepted way. The technics of the different preconditioning technics have to be investigated in several new applications.

Those technologies can create a relative rock mass rating (short rRMR). The rRMR in the tables ranges from 100 % down to 72 % of the original RMR value.

Environmental influences like dust, vibrations, heat development, moisture, water (pore water and surface water) and as well the surrounding rock pressure will increase or decrease efficiency of the performance. Those effects have to be investigated in future projects.

A possible solution could be a combination of those preconditioning technologies and roadheader with undercutting discs. Figure 52 shows such a undercutting application.
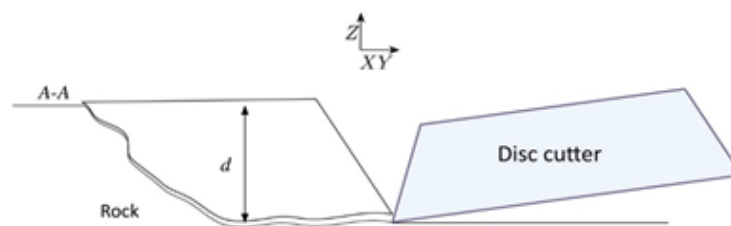
Figure 52: Disc cutter (confluence.csiro.au)

The influence of the rock mass rating also influences the planning of excavating operations. A different attack angle to the rock face could be carried out by a different position of the tunnel/drift portals. The Rating after Bieniawski will be the best application, because it unites all important parameters to one useable factor.

Out of all compared hybrid cutting models the model of Comakli shows the best fitting. The input parameters can be easy reviewed in the laboratory. After some tests the model will have to adjusted to the in situ situations. It cannot be applied in a general way in all operations. The experience of the operator will influence the performance as well.

The efficiency of microwave antennas has to be optimized to reduce the scale. A smaller scale will increase the antenna density and thereby the induced cracks will decrease the cutting forces.

8 Bibliography

Ahmadi, M.; Erfan, M. R.; Torkamany, M. J.; Safian, Gh.A. (2011): The effect of interaction time and saturation of rock on specific energy in ND. YAG laser perforating. In: *Optics & Laser Technology* 43 (1), S. 226–231. DOI: 10.1016/j.optlastec.2010.06.018.

Barton, Lien and Lunde (1974): Barton, Lien and Lunde, 1974. Engineering classification of rock masses for.

Bilgin; Dincer.; Copur; Erdogan (2004): Some geological and geotechnical factors affecting the performance of a roadheader in an inclined tunnel. In: *Tunnelling and Underground Space Technology* 19 (6), S. 629–636. DOI: 10.1016/j.tust.2004.04.004.

Celal, Irfan (2013): Theories on Rock Cutting, Grinding and Polishing Mechanisms. In: Hasim Pihtili (Hg.): Tribology in Engineering: InTech.

Comakli, Kahraman, Balci (2014): Performance prediction of roadheaders in metallic ore excavation. In: *Tunnelling and Underground Space Technology* 40, S. 38–45. DOI: 10.1016/j.tust.2013.09.009.

Graves, Ramona; Samih, Batarseh; Parker, Richard; Gahan, Brian;2002; Temperatures Induced by High Power Lasers: Effects on Reservoir Rock Strength and Mechanical Properties. In: SPE/ISRM Rock Mechanics Conference.

Graves; O'Brien l. 1998: StarWars Laser Technology Applied to Drilling and Completing Gas Wells. In: SPE Annual Technical Conference and Exhibition.

Gryc; Hlaváč; Mikoláš; Šancer; Daněk (2014): Correlation of pure and abrasive water jet cutting of rocks. In: *International Journal of Rock Mechanics and Mining Sciences* 65, S. 149–152. DOI: 10.1016/j.ijrmms.2013.11.001.

Hoek, Evert: 1 Rock mass classification. In: *Rocksience*. Online verfügbar unter https://www.rocscience.com/documents/hoek/corner/04_Rock_mass_classification.pdf.

Hoek, Carter, Diederichs (Hg.) (2013): 2013 16th International Multi Topic Conference (INMIC). Geomechanics Symposium Quantification of the Geological Strength Index Chart. Lahore, Pakistan.

Käsling, Thuro (2010): Determining rock abrasivity in the laboratory. Williams, A.L., Pinches, G.M., Chin, C.Y., McMorran, T.J. & Massey, C.I. 11th IAEG Congress. In: *Geologically active* 2010 (235), S. 1973–1980. Online verfügbar unter http://www.geo.tum.de/people/thuro/pubs/2010_eurock_abrasivity.pdf.

Liu S.; Liu, X.; Chen; Lin (2015): Rock breaking performance of a pick assisted by high-pressure water jet under different configuration modes. In: *Chin. J. Mech. Eng.* 28 (3), S. 607–617. DOI: 10.3901/CJME.2015.0305.023.

Marinos (2000): GSI: a geologically friendly tool for rock mass strength estimation.

Munoz, H.; Taheri, A.; Chanda, E. (2016): Rock cutting characteristics on soft-to-hard rocks under different cutter inclinations. In: *International Journal of Rock Mechanics and Mining Sciences* 87, S. 85–89. DOI: 10.1016/j.ijrmms.2016.05.014.

Ocak, Bilgin (2010): Comparative studies on the performance of a roadheader, impact hammer and drilling and blasting method in the excavation of metro station tunnels in Istanbul. In: *Tunnelling and Underground Space Technology* 25 (2), S. 181–187. DOI: 10.1016/j.tust.2009.11.002.

Oh; Prasidhi.; Cho; Shin (2014): Effect of water jet geometric parameters on rock fracturing. In: *KSCE J Civ Eng* 18 (3), S. 772–779. DOI: 10.1007/s12205-014-0338-0.

Paul, S.; Hoogstrate, A.M; van Luttervelt, C.A; Kals, H.J.J (1998): Analytical and experimental modelling of the abrasive water jet cutting of ductile materials. In: *Journal of Materials Processing Technology* 73 (1-3), S. 189–199. DOI: 10.1016/S0924-0136(97)00228-8.

Pihtili, Hasim (Hg.) (2013): Tribology in Engineering: InTech.

Restner; Gehring (2000): QUANTIFICATION OF ROCK MASS INFLUENCE ON CUTTABILITY WITH ROADHEADERS. In: The Zinc Industry: Elsevier, Introduction/page i-Introduction/page ii.

Tavallali, Abbass; Vervoort, André (2010): Effect of layer orientation on the failure of layered sandstone under Brazilian test conditions. In: *International Journal of Rock Mechanics and Mining Sciences* 47 (2), S. 313–322. DOI: 10.1016/j.ijrmms.2010.01.001.

Thuro, Plinninger (2002): Klassifizierung und Prognose von Leistung- und Verschleißparametern im Tunnelbau. In: *Taschenbuch für den Tunnelbau* 2002 (27), S. 62–126.

Tiryaki, Bulent (2008): Application of artificial neural networks for predicting the cuttability of rocks by drag tools. In: *Tunnelling and Underground Space Technology* 23 (3), S. 273–280. DOI: 10.1016/j.tust.2007.04.008.

Tiryaki, Bulent (2009): Estimating Rock Cuttability using Regression Trees and Artificial Neural Networks. In: *Rock Mech Rock Eng* 42 (6), S. 939–946. DOI: 10.1007/s00603-008-0012-2.

Toifl (2016): Numerical study of microwave induced stress and damage formation in heterogeneous rocks. In: *Doctoral Thesis, Montanuniveritaet Leoben*.

Tumac; Bilgin; Feridunoglu; Ergin (2007): Estimation of Rock Cuttability from Shore Hardness and Compressive Strength Properties. In: *Rock Mech. Rock Engng.* 40 (5), S. 477–490. DOI: 10.1007/s00603-006-0108-5.

Wickham; Tiedemann; Skinner: Support determination based on geologic predictions. American Institute of Mining, Metallurgical and Petroleum Engineers (AIME), New York. pp. 43–64. In: *In Lane, K.S.; Garfield, L.A. Proc. 1st North American Rapid Excavation & Tunnelling Conference (RETC), Chicago* 1972.

Yagiz; Gokceoglu. (2010): Application of fuzzy inference system and nonlinear regression models for predicting rock brittleness. In: *Expert Systems with Applications* 37 (3), S. 2265–2272. DOI: 10.1016/j.eswa.2009.07.046.

Yasar; Erdogan (2004): Estimation of rock physicomechanical properties using hardness methods. In: *Engineering Geology* 71 (3-4), S. 281–288. DOI: 10.1016/S0013-7952(03)00141-8.

Yilmaz; Tumac; Goktan (2015): Rock cuttability assessment using the concept of hybrid dynamic hardness (HDH). In: *Bull Eng Geol Environ* 74 (4), S. 1363–1374. DOI: 10.1007/s10064-014-0692-7.

9 List of figures

10 List of tabels

11 List of equations

---

12 Annex

12.1 Ocak and Bilgin (laser cutting)

Most of the prediction models show a to high cutting performances, but to show the influence of hybrid cutting to them, some of those are presented in this part of the thesis.

Equation 39 was used to calculate the hybrid cutting ICR out of the original ICR.

First will be the Ocak and Bilgin hybrid cutting application for axial roadheader:

Table 18: Laser hybrid cutting axial Ocak and Bilgin

UCS	RMCI	Original ICR	hybrid cutting ICR
75	61.91	16.44	20.02
100	82.54	9.54	11.62
125	103.18	5.54	6.75
150	123.82	3.21	3.92
175	144.45	1.86	2.60
200	165.09	1.08	1.51
225	185.73	0.63	0.87
250	206.37	0.36	0.51

Depending on a different cutting depth and preconditioning situation a difference between 21.8 % and 39.5 % of the ICR could be achieved.
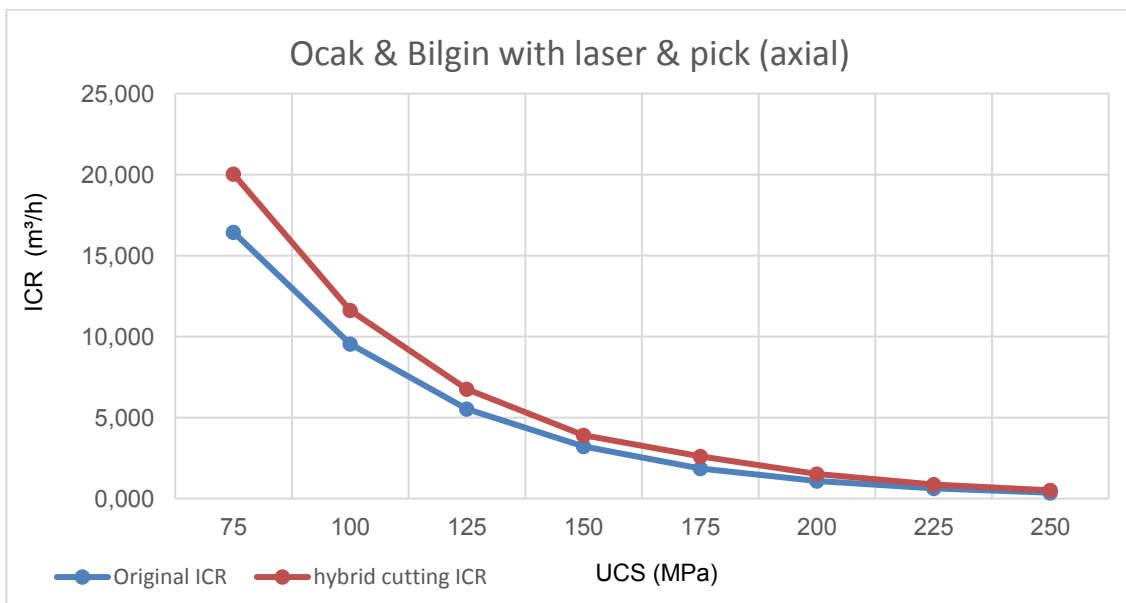

Figure 53: Hybrid cutting axial Ocak and Bilgin model (laser)

Second will be the Ocak and Bilgin application for transversal roadheader:

Equation 39 was used to calculate the hybrid cutting ICR out of the original ICR.

Table 19: Laser hybrid cutting model transversal Ocak and Bilgin

UCS	RPI	Original ICR	hybrid cutting ICR
75	296.00	53.6	65.2
100	222.00	45.2	55.0
125	177.60	40.8	49.7
150	148.00	38.1	46.4
175	126.86	36.3	50.7
200	111.00	35.0	48.8
225	98.67	34.0	47.5
250	88.80	33.3	46.4

Depending on a different cutting depth and preconditioning situation a difference between 21.8 % and 39.5 % of the ICR could be achieved.
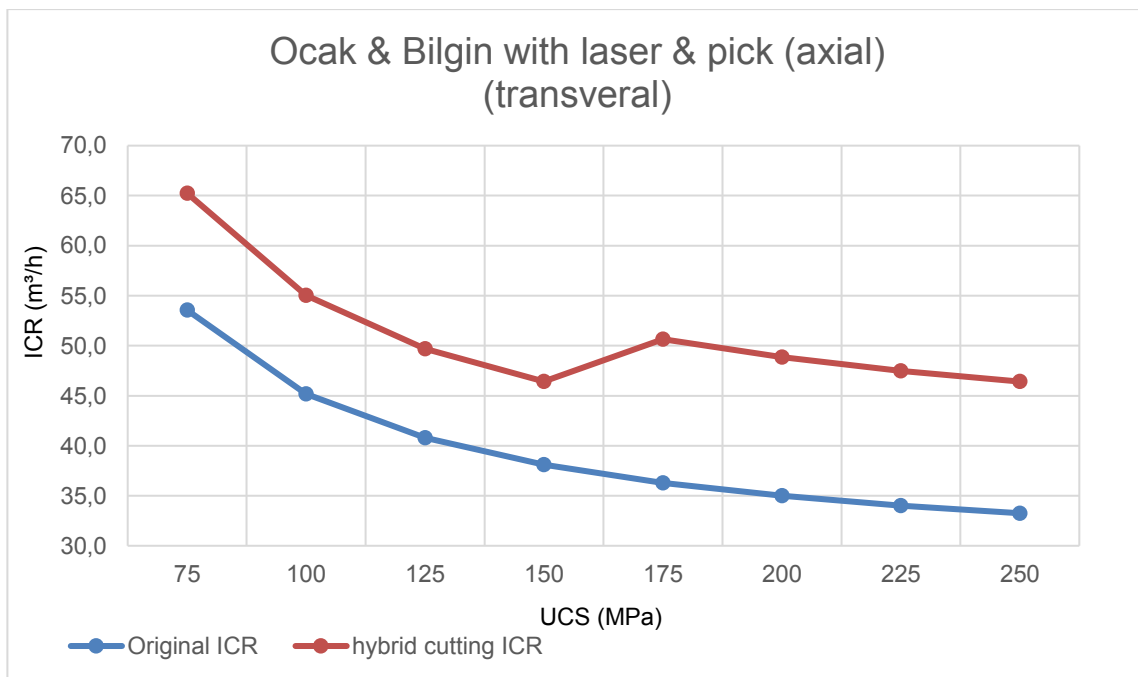

Figure 54: Hybrid cutting Ocak and Bilgin model (laser)

12.2 Ocak and Bilgin (microwave)

First in this chapter will be the situation for axial cutting roadheaders.

Equation 39 was used to calculate the hybrid cutting ICR out of the original ICR.

Table 20: Microwave hybrid cutting axial Ocak and Bilgin

UCS	RMCI	Original ICR	hyprid cutting ICR
75	61.91	16.44	20.40
100	82.55	9.55	11.84
125	103.19	5.54	6.88
150	123.82	3.22	3.99
175	144.46	1.87	2.56
200	165.10	1.08	1.48
225	185.73	0.63	0.86
250	206.37	0.37	0.50

Depending on a different cutting depth and preconditioning situation a difference between 24.1 % and 36.7 % of the ICR could be achieved.
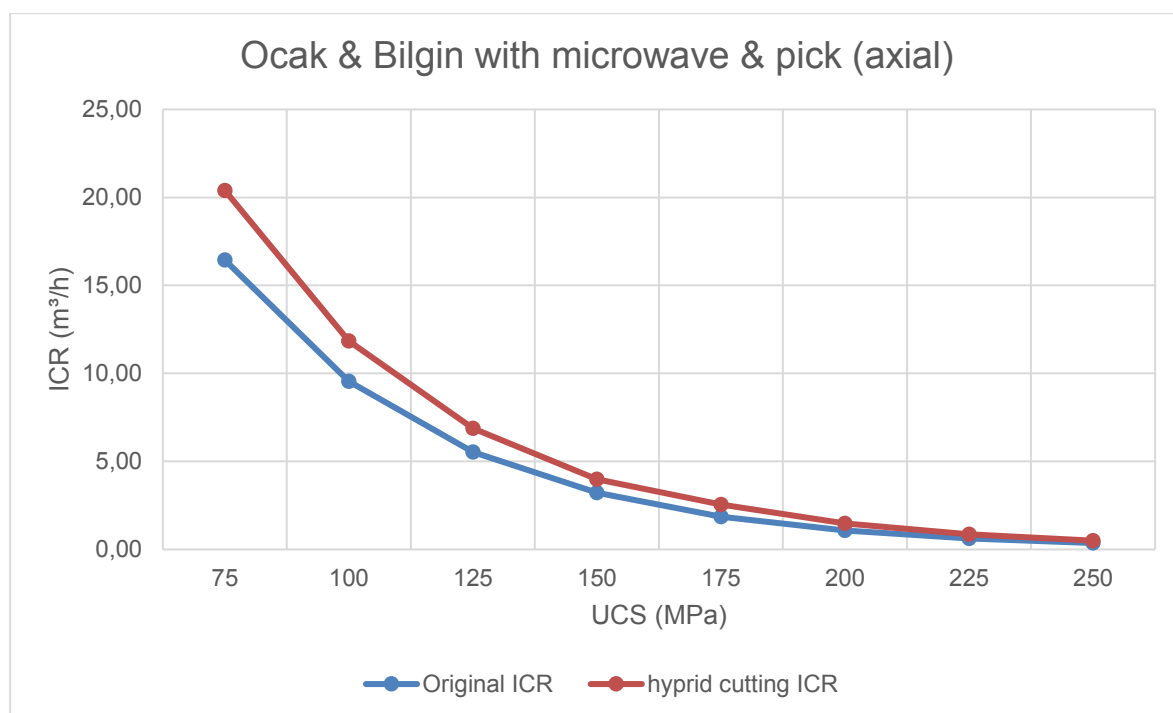

Figure 55: Hybrid cutting axial Ocak and Bilgin model (microwave)

Second will be the situation for transversal cutting roadheaders:

Equation 39 was used to calculate the hybrid cutting ICR out of the original ICR.

Table 21: Microwave hybrid cutting transversal Ocak and Bilgin

UCS	RPI	Original ICR	hyprid cutting ICR
75	296.00	53.6	65.2
100	222.00	45.2	55.0
125	177.60	40.8	49.7
150	148.00	38.1	46.4
175	126.86	36.3	49.6
200	111.00	35.0	47.9
225	98.67	34.0	46.5
250	88.80	33.3	45.5

Depending on a different cutting depth and preconditioning situation a difference between 21.4 % and 36.7 % of the ICR could be achieved.
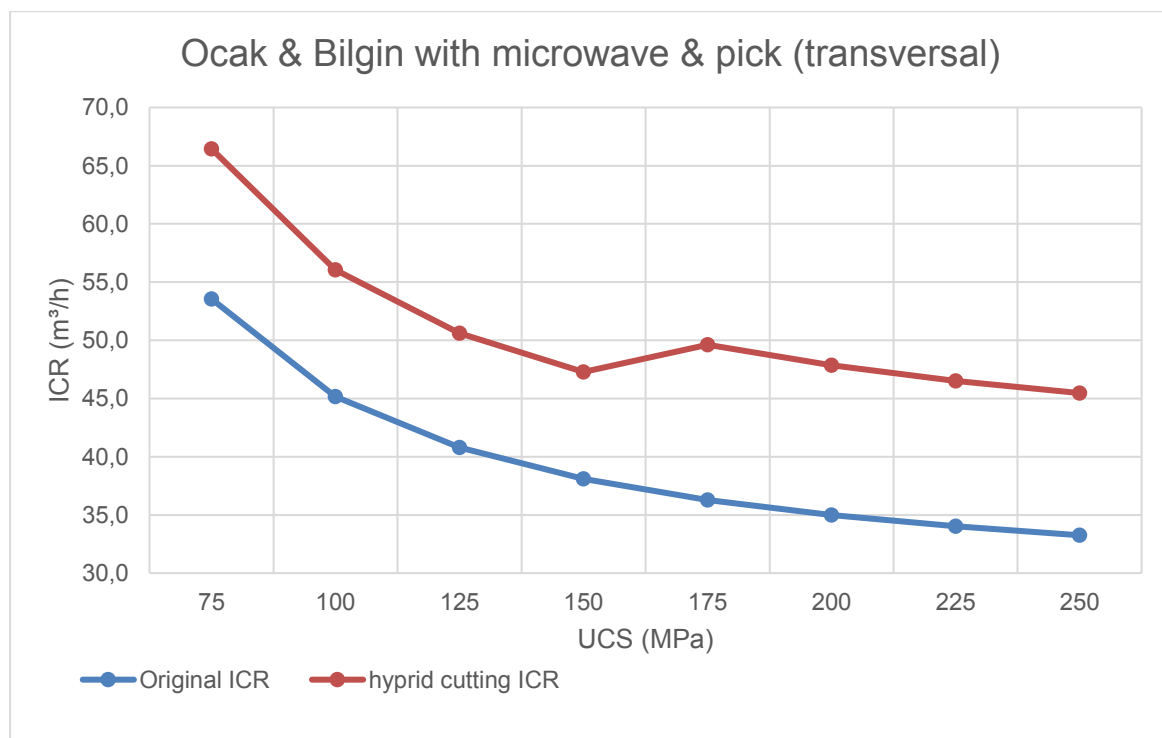

Figure 56: Hybrid cutting transversal Ocak and Bilgin model (microwave)